THE USE OF A NON-CLASSICAL FRICTION LAW IN FINITE-ELEMENT ANALYSIS OF CONTACT PROBLEMS

by

A.C. BOLT

A Thesis submitted in partial fulfillment of the requirements for the degree of Master of Science (Engineering)

Department of Civil Engineering
University of Cape Town

September 1983

DECLARATION OF CANDIDATE

I hereby declare that this thesis is my own work and that it has not been submitted for a degree at any other university.

Signed by candidate

A.C. BOLT

ACKNOWLEDGEMENTS

I wish to express my thanks to the following :

Dr. B.D. Reddy, who suggested the topic and supervised the research;

Professor J.B. Martin, for helpful discussion;

The NLSMRU, for the use of NOSTRUM version 2.4 ;

Mrs. G. King, for typing this thesis;

The C.S.I.R., for their financial support;

Mr. H. Cable, for printing this thesis.

ABSTRACT

In this thesis a description is given of the numerical treatment of contact problems in elasticity. Frictional effects on the contact surface are modelled by using a nonlocal, nonlinear friction law. Features of the boundary value problem, which merit special attention, are the presence of inequality constraints and the fact that the contact surface is not known a priori. Finite element approximations based on a variational formulation of the problem, developed by Oden and Pires [1], are used to generate a discretised version. The solution procedure incorporates an iterative algorithm for the determination of the extent of the contact surface. Alternative techniques for the evaluation of the frictional stresses on the contact surface are described and numerical examples are presented.

TABLE OF CONTENTS PAGE

TABLE OF CONTENTS (Continued ...) PAGE

SYMBOLS AND NOTATION

$a(\underline{u},\underline{v})$	-	virtual work produced by action of stress $\sigma_{\alpha\beta}(\underline{u})$ on strains caused by the displacement $\underline{v}$.
$E_{\alpha\beta\gamma\partial}$	-	fourth order tensor of elastic moduli.
$f(\underline{v})$	-	virtual work done by the external forces.
$\{F\}$	-	load vector.
$\{\hat{F}\}$	-	frictional force vector.
h_i	-	shape functions for node i.
$I_\varepsilon(\underline{v})$	-	energy functional.
$j_{\rho,\varepsilon}(\underline{u},\underline{v})$	-	the virtual work of the frictional forces on the displacement $\underline{v}$.
J	-	Jacobian matrix.
$[k]$	-	stiffness matrix.
K	-	subset of V consisting of all displacements $\underline{v}$ in V for which $\underline{v}.\underline{n} \leq s$
ℓ^e	-	length of element frictional edge.
n_α	-	component of outward normal vector to boundary.
N	-	normal force.
N_f	-	order of gaussian integration.
N_g	-	number of gauss points in an element.

s	-	initial gap between elastic body and rigid boundary.
S_ρ	-	convolution of ω_ρ and σ_n.
t_α	-	component of tangent vector to boundary.
T_e	-	mapping function from master element to element in body.
T	-	tangential force.
u_t	-	tangential displacement along the boundary $= u_\alpha t_\alpha$.
u_α	-	components of the displacement field.
$\{u\},\{v\}$	-	displacement vectors.
V	-	space of admissible displacements.
w_A	-	gaussian weight factor.
(x,y)	-	cartesian co-ordinates.
Γ_C	-	area of possible contact.
Γ_{C^*}	-	area of actual contact.
Γ_D	-	area on which displacements are prescribed.
Γ_F	-	area on which tractions are prescribed.
ε	-	nonlinear parameter.
ν	-	coefficient of friction.
(ξ,η)	-	natural co-ordinates.
ρ	-	nonlocal parameter.
σ_n	-	normal component of surface traction.

σ_t - tangential component of surface traction.

$\sigma_{\alpha\beta}$ - components of stress tensor.

τ - prescribed tangential stress.

ϕ_ε - nonlinear weight function.

ψ_ε - primitive of ϕ_ε : $\phi_\varepsilon = \psi_\varepsilon'$

ω_ρ - nonlocal weight function.

Ω - subset of $\mathbb{R}^3$ occupied by elastic body.

Ω^e - element (e) in elastic body.

$\hat{\Omega}$ - master element.

Subscripts and Superscripts

Tensor notation with the normal summation convention is used and Greek subscripts $\alpha,\beta,\ldots$ (range 1 to 2) are reserved for components of tensors.

i,j,... - node numbers.

A,B,... - gauss points.

(k) - denotes the k-th iteration.

e - denotes element e.

CHAPTER 0

INTRODUCTION

The first successful attempt at an analysis of the theory of contact between elastic bodies was by Hertz [4], who investigated the contact between two elastic bodies. A solution was obtained in the form of a potential which described the stress and deformation near the contact point as a function of the geometrical and elastic properties of the bodies. The result, although both static and elastic in nature, has been widely applied to contact situations where permanent deformations were produced. The use of the Hertz law beyond the limits of its validity has been justified, on the basis that it appears to predict accurately most of the contact parameters that can be measured experimentally. This law and its various extensions [5,6] are based on the assumption that contact is frictionless. Other problems worth mentioning are those involving indentation of half-spaces by punches having various geometries; such problems are discussed by Green and Zerna [19], amongst others.

The inclusion of Coulomb friction results in a considerably more complex problem which lends itself quite naturally to investigation via the theory of variational inequalities. This theory has been developed in Italy and France by Signorini (1959), Fichera (1964) and Duvaut and Lions (1976)[7-9]. This school uses advanced functional analytic tools and lays emphasis on theoretical development: for instance, Duvaut and Lions[9] confine themselves to existence and uniqueness theorems.

In contrast, Kalker [10-13]; Singh and Paul [16], and Conry and Seireg [17] have developed a numerical solution of contact problems using weak or variational formulations. Various solutions are given by Kalker [14,15] and by Francavilla and Zienkiewicz [18] for different types of problems.

In the case of contact between a rigid body and an elastic body, it is normally assumed either that contact is frictionless or that the classical Coulomb law of static dry friction holds. However, both mathematical and numerical difficulties arise when Coulomb's law is applied pointwise to boundary value problems of elasticity. This has resulted in the development of a non-classical friction law by Oden and Pires [1] which takes into account the normal stress in the vicinity of a point (this is called the nonlocal effect), and the elastic deformation prior to gross sliding (known as the nonlinear effect). In reference [1], the non-classical law is developed in detail and variational principles are derived for boundary value problems in elasticity which use this law.

The aim of this thesis is to make use of some of the principles derived in [1] in order to obtain approximate solutions to contact problems in elasticity which make use of the non-classical friction law.

The plan of the thesis is as follows:
In Chapter One an account is given of the theory underlying the nonlocal nonlinear friction law. The set of governing equations and inequalities for a contact problem in elasticity with the non-classical friction are then formulated; a variational inequality is given, which reduces to a variational

equality when the tangential stress is assumed prescribed. This formulation is used subsequently in the numeric implementation.

In Chapter Two, the variational equality is formulated in a finite-dimensional subspace, using the finite element method. This results in a set of equations of the form

$$\{v\}^T[k]\{u\}+\{v\}^T\{\hat{F}\} = \{v\}^T\{F\}$$

where the term $\{\hat{F}\}$ arises as a result of the frictional forces. This term is nonlinear as it depends on the extent of the contact area and on the normal stress, both of which are not known a priori. This necessitates the use of an iterative algorithm for the solution of the contact problem.

Chapter Three describes this algorithm. The iterative process is initiated by making an initial guess of the contact area Γ_{C*} and by assuming that the contact is frictionless. After each iteration, the contact area Γ_{C*} and tangential stress are updated in a suitable manner.

Various examples are presented and discussed in Chapter Four. There are two plane strain examples, a rectangular punch and a cylindrical punch on its side, both indenting an elastic half-space; two axisymmetric examples, an annular punch and a cylindrical punch on its end, both indenting elastic half-spaces; and finally, a plane stress example of a thin sheet being pulled through a gap.

The thesis concludes with a discussion of various important features related to the friction law which are evident in the examples presented; possible extensions and improvements of the present scheme are also discussed.

CHAPTER 1

1. FORMULATION OF THE NONLOCAL NONLINEAR FRICTION LAWS

1.1 Coulomb's Friction Law

The classical Coulomb law of static dry friction states that:

> Relative sliding between two bodies in contact along plane surfaces will occur when the nett shear force (T) parallel to the plane reaches a critical value proportional to the nett normal force (N) pressing the bodies together. The constant of proportionality is called the coefficient of friction (ν).

This law is illustrated in Figure (1.1). If N and T are the normal and tangential forces respectively, then,

$$\begin{aligned} &\text{if} \quad |T| < \nu N \ , \quad |u_t| = 0 \\ &\text{if} \quad |T| = \nu N \ , \quad \text{there exists a } \lambda \geq 0 \text{ such} \\ &\qquad\qquad\qquad \text{that } |u_t| = \lambda |T| \end{aligned} \qquad \ldots [1.1]$$

where $|u_t|$ is the magnitude of the displacement tangential to the plane in the direction of the tangential force T.

This law is unsatisfactory in many respects when used in boundary value problems of elasticity, because:

(i) the law is formulated pointwise and does not take into account the effects of normal tractions in adjacent regions; thus this law does not model variations in surface roughness;

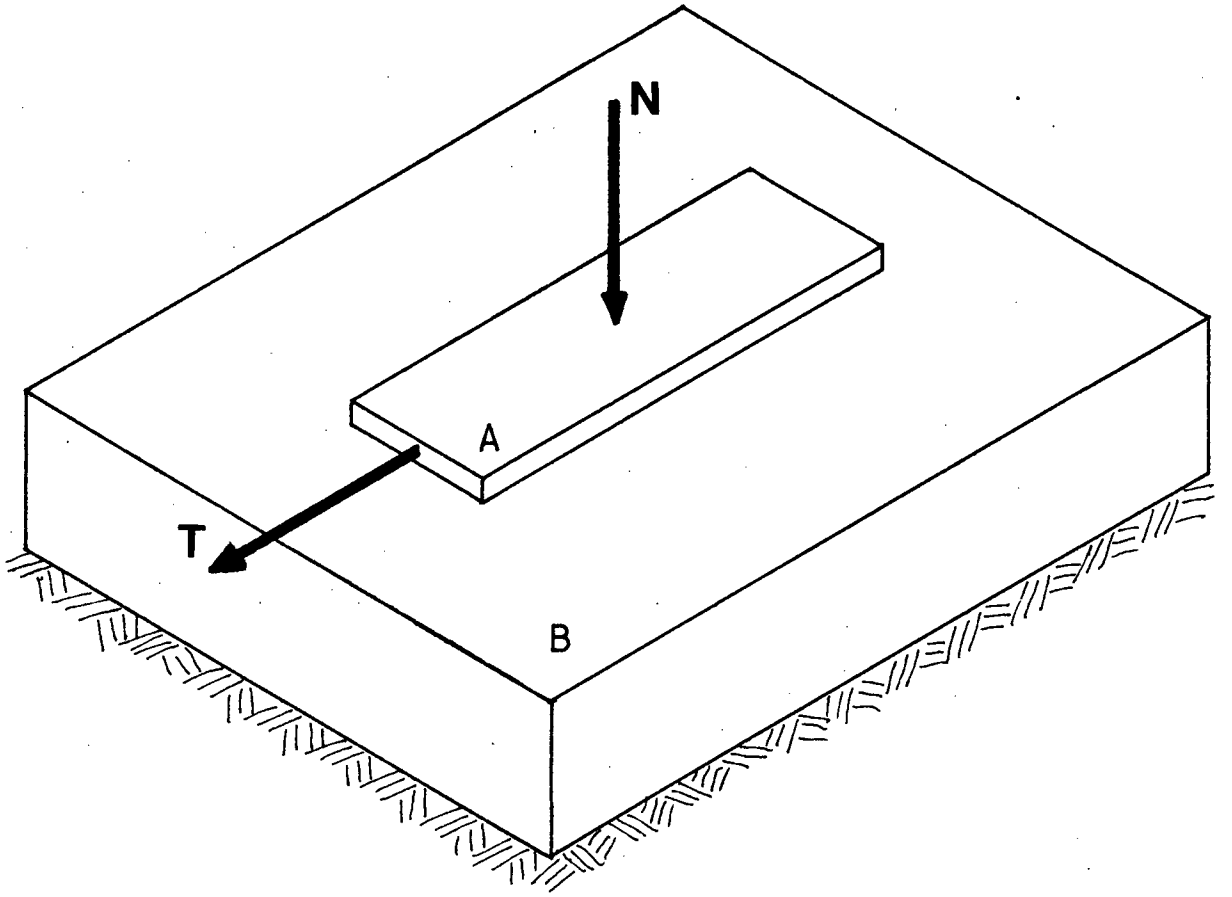

Figures: 1.1(a) Two bodies A and B pressed together with forces N and T applied to body A.

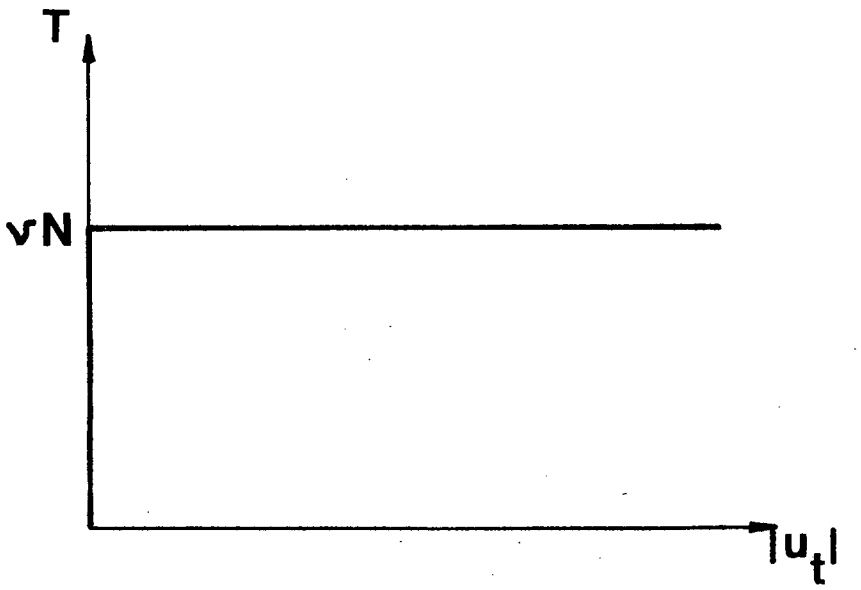

(b) The Coulomb friction relationship between T and u_t

(ii) there is no guarantee that a solution exists when this friction law is used in boundary value problems of elasticity;

(iii) physically this law was only intended to be applied to rigid bodies undergoing gross sliding, with the boundary not being modelled by discrete points.

These problems with Coulomb's friction law motivated the formulation of a nonlocal nonlinear friction law by Oden and Pires [1]. In Section 1.2 this generalization is discussed.

1.2 The Nonlocal Nonlinear Friction Law

Consider two bodies in contact with forces which are tangential and normal to the plane of contact acting on them (see Figure 1.2(a)). The contact planes prior to contact, when observed on a micro-scale, consist of many irregular asperities (see Figure 1.2(b)). When contact is made, these asperities deform and fuse forming junctions which effectively bond the two surfaces together (see Figure 1.2(c)). When a tangential stress is applied along the contact plane, there is some tangential movement attributed to the tangential stiffness of the bond prior to the fracture of the bond (see Figure 1.2(d)). Gross sliding occurs once this bond has fractured.

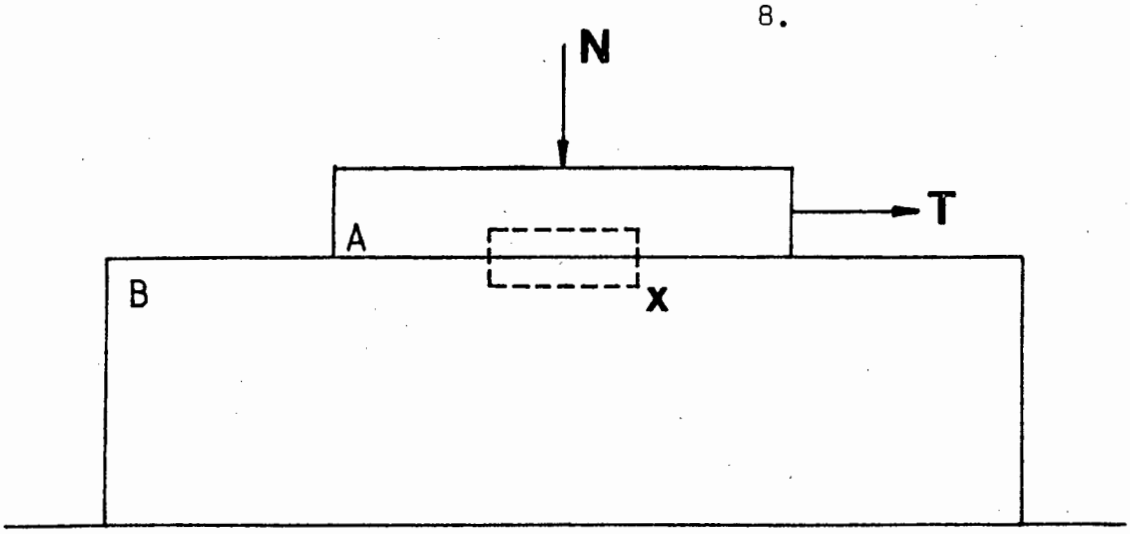

Figures: 1.2(a) Two bodies A and B in contact.

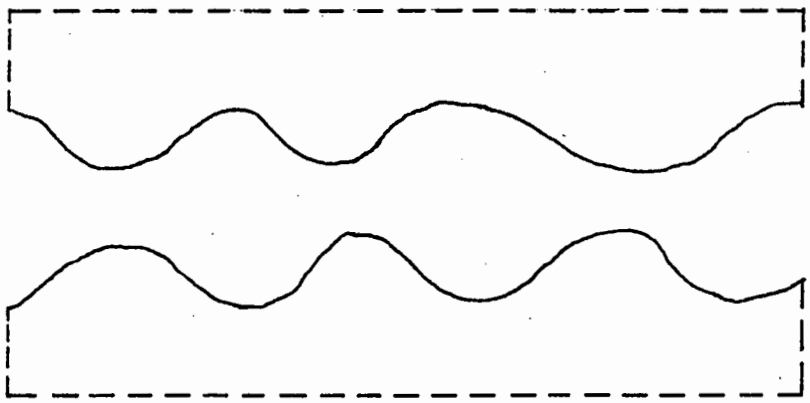

(b) Detail X before contact has been made.

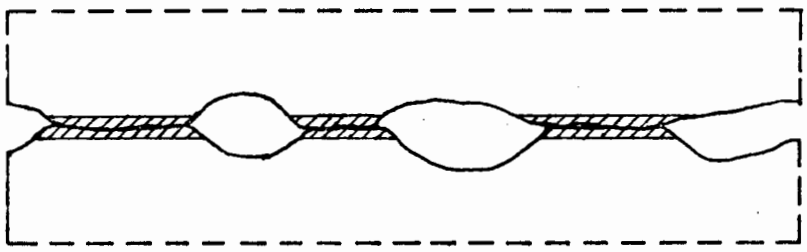

(c) Detail X once A and B are in contact.

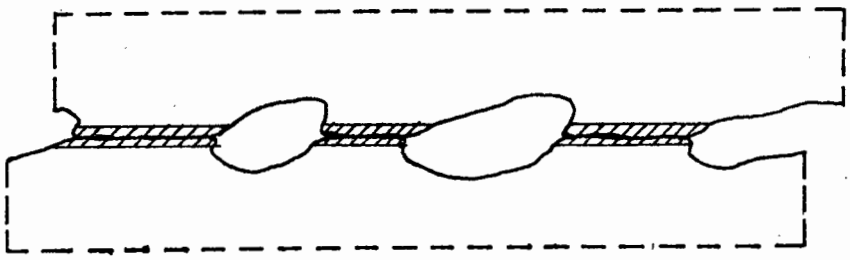

(d) Detail X showing the tangential displacement before gross sliding.

Three parameters are required in order to model the above behaviour:

ν - coefficient of friction which is associated with the gross sliding between the two bodies;

ρ - a roughness related parameter representing the nonlocal character of the junction. If the asperities are assumed to be spherical then ρ would be equal to the radius of the fused junction;

ε - a measure of the tangential stiffness of the elastic behaviour of the junction. This represents the nonlinear part of the friction law.

If $\rho \to 0$ (local) and $\varepsilon \to 0$ (fully rigid (linear)), this law reverts to Coulomb's friction law.

The nonlocal and then the nonlinear aspects of this frictional behaviour will now be examined in greater detail.

1.2.1 The Nonlocal Friction Law

This law states:

> Impending motion at a point of contact between two deformable bodies will occur when the shear stress at that point reaches a value proportional to a weighted measure of the normal stresses in the neighbourhood of the point . [1]

This weighting must be such that it is a maximum where the force is centred, tapering out to zero at the edges of the

contact area. A simple weighting function which would fit this condition would be a negative parabola with its peak where the force is centred. Another function, the one used later in the implementation of this law in a computer program, is the bell-shaped function $\omega_\rho(x)$, which is defined by:

$$\omega_\rho(x) = Ce^{\frac{\rho^2}{x^2-\rho^2}} \quad \text{if} \quad |x| \leq \rho$$
$$= 0 \quad \text{if} \quad |x| > \rho \qquad \ldots.[1.2]$$

Where C is a constant with dimensions of $(\text{length})^{-2}$ (see Figures 1.3(a) and (b)) such that $\omega_\rho(0)=1$.

The nonlocal law thus states that gross sliding occurs at a point when the tangential surface stress at that point reaches a value defined by the equation. (1.3)

$$\sigma_t(x) = \nu \int_{-\rho}^{\rho} \omega_\rho(|x-y|)\, \sigma_n(y)\, dy \qquad \ldots.[1.3]$$

Where $\sigma_n = \sigma_{\alpha\beta} n_\alpha n_\beta$ is the normal component of the stress tensor $\sigma_{\alpha\beta}$ evaluated at the point x on the boundary, and $\sigma_t = \sigma_{\alpha\beta} t_\alpha t_\beta$ is the tangential component of the stress tensor $\sigma_{\alpha\beta}$ evaluated using (1.3) at the point x on the boundary.

For future reference let the above convolution be referred to as $S_\rho(x)$, that is,

$$S_\rho(x) = \omega_\rho * \sigma_n$$
$$= \int_{-\rho}^{\rho} \omega_\rho(|x-y|)\, \sigma_n(y)\, dy \qquad \ldots.[1.4]$$

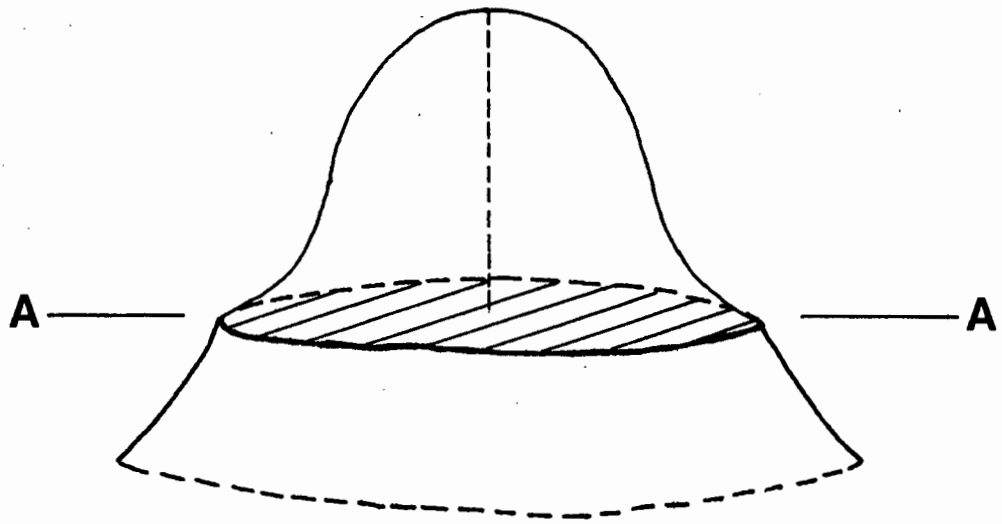

Figures: 1.3(a) An ω_ρ distribution over the asperity contact area.

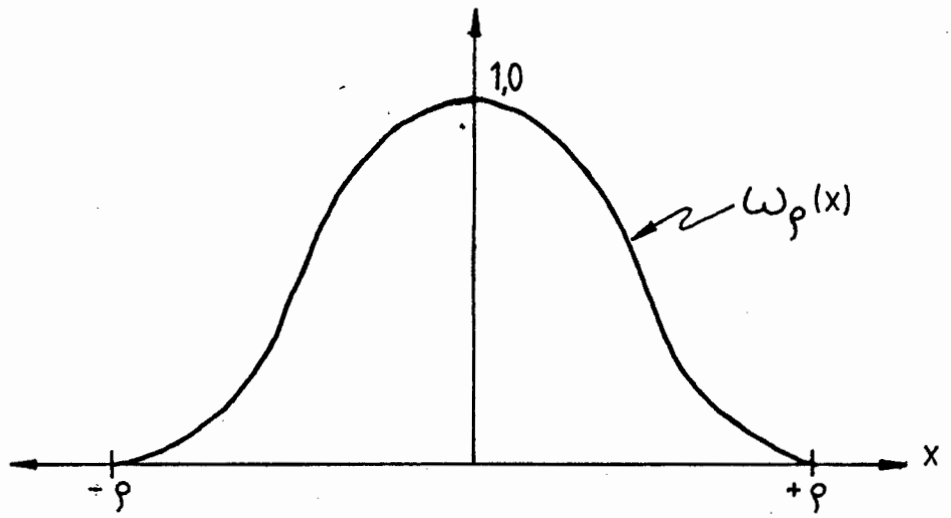

(b) A vertical section through A-A in Figure 1.3(a).

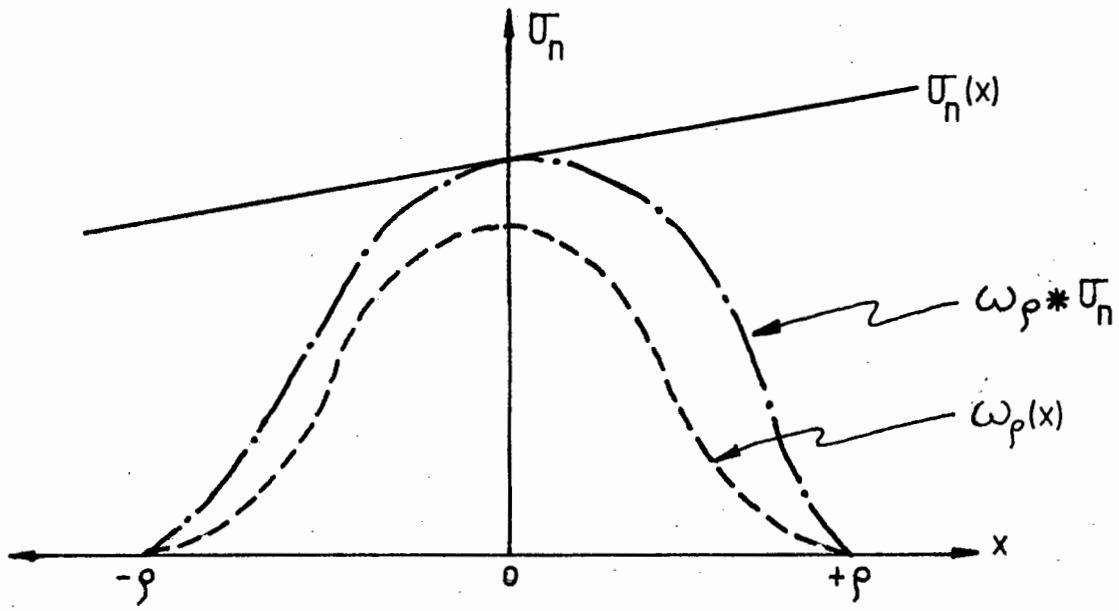

(c) The effect of ω_ρ on a linear σ_n

The effect of this weighting factor on the normal stress is shown in Figure 1.3(c).

Coulomb's friction law (1.1) can now be altered to accommodate this nonlocal effect. Thus the nonlocal friction law is:

$$\text{if } |\underline{\sigma}_t(\underline{u})| < \nu S_p(\sigma_n(\underline{u})) \quad \text{then } \underline{u}_t = \underline{0}$$

$$\text{if } |\underline{\sigma}_t(\underline{u})| = \nu S_p(\sigma_n(\underline{u})) \quad \text{then there exists a } \lambda \geq 0 \text{ such that}$$

$$\underline{u}_t = -\lambda \underline{\sigma}_t \qquad \ldots.[1.5]$$

Here, $\underline{u}$ is the displacement vector at a point on the boundary, and the expression $\sigma_n(\underline{u})$ indicates that σ_n is evaluated using the elastic constitutive law. That is,

$$\sigma_n = \sigma_{\alpha\beta} n_\alpha n_\beta$$

$$= E_{\alpha\beta\gamma\partial} u_{\gamma,\partial}$$

where $E_{\alpha\beta\gamma\partial}$ is the fourth order tensor of elastic moduli and a subscript following a comma denotes partial differentiation with respect to the corresponding component.

The nonlocal law still assumes that there is only gross sliding, and that there is no elastic deformation at the junctions prior to sliding. In other words, there is an abrupt transition from sticking to sliding. Through the introduction of the nonlinear law this abrupt transition is removed. The nonlinear law models the small scale relative displacement across the junction prior to gross sliding; this is discussed next.

1.2.2 The Nonlinear Friction Law

The nonlinear friction law incorporates the elastic deformation prior to fracture and gross sliding across a junction, into the friction law as stated in (1.5). The bonds created between asperities which have come into contact must be broken before gross sliding can occur. There is some tangential displacement prior to this due to the deformation of the junction, and the amount is dependent on the strength or stiffness of the junction. This phenomenon can be modelled by a family of nonlinear functions denoted by $\phi_\varepsilon(r)$, (r being a measure of the tangential displacement) with the following properties:

(i) they must be continuous, monotone, real valued, non-negative, and dependent on the tangential stiffness parameter ε ;

(ii) they must be within the limits of

$$0 \leq \phi_\varepsilon(r) \leq 1 \quad \text{for all } r \geq 0$$

(iii) the $\lim_{\varepsilon \to 0} \phi_\varepsilon(r) = 1$ must exist for all $r > 0$

(iv) the $\lim_{r \to \infty} \phi_\varepsilon(r) = 1$ must exist for all $\varepsilon > 0$ ....[1.6]

There are many curves which fit this description, of which two are:

(a) $$\phi_\varepsilon(|\underline{u}_t|) = \tanh \frac{(|\underline{u}_t|)}{\varepsilon}$$ ....[1.7a]

$$\text{(b)} \quad \phi_\varepsilon(|\underline{u}_t|) = 1 \qquad \text{if} \quad |\underline{u}_t| > \varepsilon$$

$$= \frac{|\underline{u}_t|}{\varepsilon} \qquad \text{if} \quad |\underline{u}_t| \leq \varepsilon \qquad \ldots.[1.7b]$$

where $\underline{u}_t$ is the component of the displacement vector at a point on the boundary tangential to the plane of contact at that point. The nonlinear function ϕ_ε is a function of the magnitude of $\underline{u}_t$ (see Figure 1.4).

Curve (b) is the curve used in the implementation of this law in the finite element approximation later on.(see Chapter 2).

The expressions in (1.5) can now be condensed into one expression with the incorporation of the function ϕ_ε, we thus have

$$\underline{\sigma}_t(\underline{u}) = - \nu S_\rho(\sigma_n(\underline{u})) \phi_\varepsilon(\underline{u}_t). \frac{\underline{u}_t}{|\underline{u}_t|} \qquad \ldots.[1.8]$$

If a one dimensional piecewise linear boundary is used, (1.8) can be simplified and becomes

$$\underline{\sigma}_t(\underline{u}(s)) = \underline{\sigma}_t(s) = - \nu S_\rho(\sigma_n(s)) \phi_\varepsilon(|\underline{u}_t|) \qquad \ldots.[1.9]$$

where s is measured along the boundary.

If $\rho \to 0$ (local) and $\varepsilon \to 0$ (fully rigid (linear)) then (1.9) degenerates to the Coulomb friction law, that is,

if $|\underline{\sigma}_t(x)| < \nu|\underline{\sigma}_n(x)|$ then $|\underline{u}_t| = \underline{0}$

if $|\underline{\sigma}_t(x)| = \nu|\underline{\sigma}_n(x)|$ then there exists a $\lambda \geq 0$ such that $|\underline{u}_t| = \lambda|\underline{\sigma}_t(x)|$

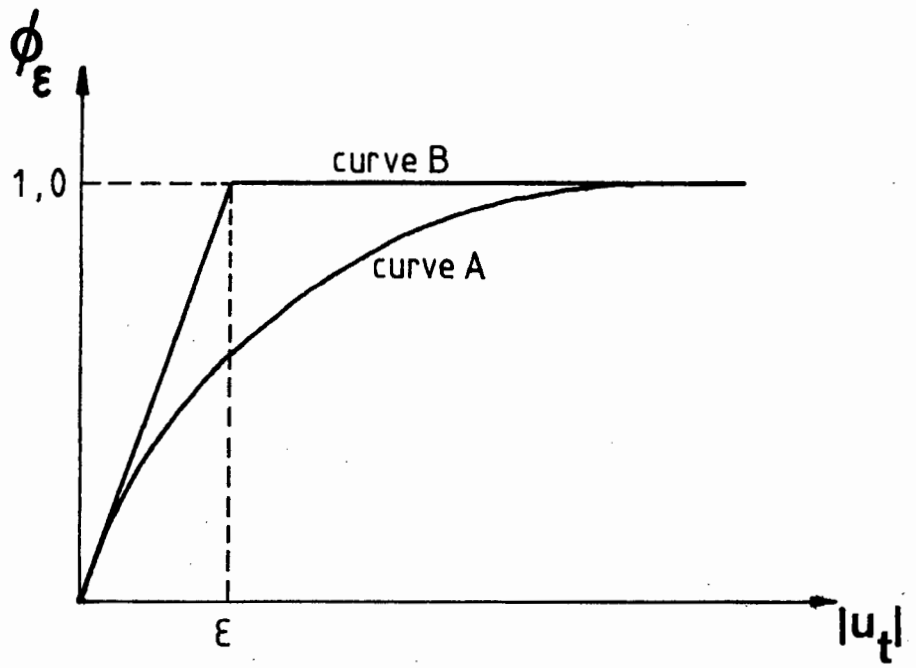

Figure 1.4 Graphs of functions 1.7(a) and 1.7(b).

The expression (1.9) is the nonlocal nonlinear friction law for a one dimensional piecewise linear boundary.

We now look at the formulation of a boundary value problem which incorporates this nonlocal nonlinear friction law.

1.3 Formulation of the Boundary Value Problem

Consider the Signorini problem of a linear elastic body Ω as shown in Figure (1.5) whose boundary Γ has three distinct areas:

(i) Γ_D - the portion of the boundary where there are prescribed displacements,

(ii) Γ_F - the portion of the boundary where there are prescribed tractions,

(iii) Γ_C - the portion of the boundary which is likely to come into contact with a rigid boundary F.

The external forces applied to the body are the surface tractions $\underline{t}(s)$, applied along Γ_F, and the body forces $\underline{f}(\underline{x})$ applied over the volume of the body.

The Signorini problem of a linear elastic body with nonlocal nonlinear friction consists of seeking a displacement field $\underline{u}$ which satisfies the following equations and inequalities:

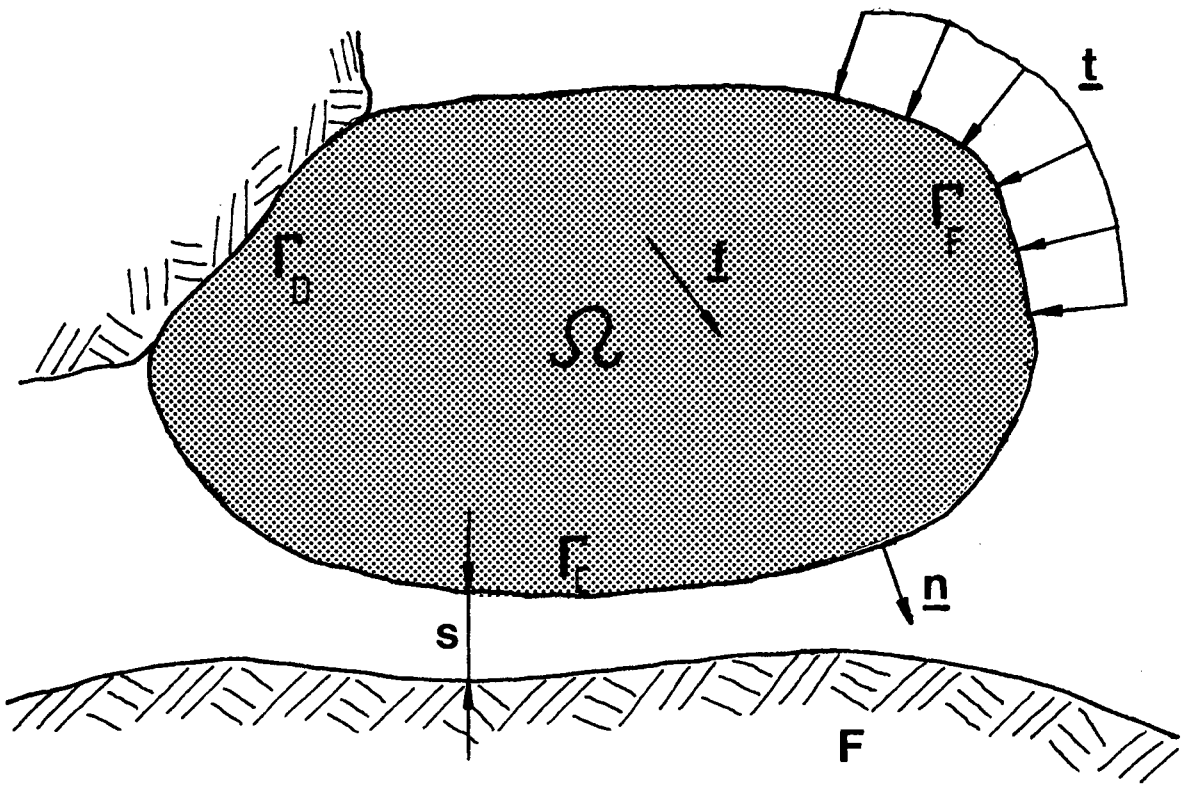

Figure 1.5 An elastic body Ω which may come into contact with the rigid rough boundary F.

(1) Constitutive equations:

Since the body is assumed to be linearly elastic, Hooke's law holds, that is,

$$\sigma_{\alpha\beta} = E_{\alpha\beta\gamma\partial} \cdot u_{\gamma,\partial} \qquad \ldots.[1.10]$$

where $E_{\alpha\beta\gamma\partial}$ is a fourth order tensor of elastic moduli:

(2) Equilibrium equations:

$$(\sigma_{\alpha\beta}(\underline{u}))_{,\beta} + f_\alpha = 0 \quad ;$$

using (1.10), can be rewritten as

$$(E_{\alpha\beta\gamma\partial}\, u_{\gamma,\partial})_{,\beta} + f_\alpha = 0 \qquad \ldots.[1.11]$$

where the subscript β following a comma implies the partial derivative with respect to x_β;

(3) Boundary conditions:

(a) Prescribed displacements:

Displacements are prescribed along Γ_D in Figure (1.5). Γ_D is assumed to be rigidly fixed, so that

$$u_\alpha = 0 \quad \text{on} \quad \Gamma_D \qquad \ldots.[1.12]$$

(b) Prescribed tractions:

The tractions along Γ_F can be written as

$$\sigma_{\alpha\beta}(\underline{u}) n_\alpha = t_\beta$$

where $\sigma_{\alpha\beta}(\underline{u})$ is the stress obtained using (1.10) and n_α are the components of the outward normal along Γ_F. t_β are the tractions prescribed along Γ_F. Substituting Hooke's law (in 1.10) the prescribed tractions are thus

$$(E_{\alpha\beta\gamma\partial} \cdot u_{\gamma,\partial}) n_\alpha = t_\beta \qquad \text{on } \Gamma_F \qquad \ldots.[1.13]$$

(c) Unilateral constraints:

Along Γ_C is a gap (s) between the body (Ω) and the rigid foundation (F). The relationship between the body's displacement ($\underline{u}$) and (s) is

$$(\underline{u}).(\underline{n}) \leq s \text{ on } \Gamma_C$$

When $\underline{u}.\underline{n} = s$ the body is in contact with the boundary (F) and $\underline{\sigma}_n(\underline{u}) \leq 0$. When $\underline{u}.\underline{n} < s$ there is no contact which implies $\underline{\sigma}_n(\underline{u}) = 0$ where

$$\underline{\sigma}_n(\underline{u}) = (E_{\alpha\beta\gamma\partial}\, u_{\gamma,\partial}) n_\alpha n_\beta$$

Thus the unilateral constraints on the contact surface Γ_C can be described concisely as follows:

$$\underline{u}.\underline{n} - s \leq 0 \qquad \underline{\sigma}_n(\underline{u}) \leq 0$$

and $\underline{\sigma}_n(\underline{u}).(\underline{u}.\underline{n} - s) = 0 \quad \text{on } \Gamma_C \qquad \ldots.[1.14]$

Finally,

(d) Friction conditions along Γ_C:

as formulated in the previous section are

$$\underline{\sigma}_t(\underline{u}) = -\nu S_\rho(\sigma_n(\underline{u}))\, \phi_\varepsilon(\underline{u}_t) \frac{\underline{u}_t}{|\underline{u}_t|} \text{ on } \Gamma_C \quad \ldots.[1.15]$$

where $S_\rho(\sigma_n(\underline{u})) = \int_{\Gamma_C} \omega_\rho(|x-y|)(\sigma_n(\underline{u}(y)))\, ds$

and ω_ρ and ϕ_ε are as defined by (1.2) and (1.7) respectively.

With the Signorini problem with nonlocal nonlinear friction formulated, a variational principle for this problem can now be established. The relationship between the variational and classical formulation can also be established.

1.4 Formulation of the Variational Principle

The following notation is used in the formulation of the variational principle:

V = space of admissible displacements. A displacement vector $\underline{v}$ will belong to V if and only if, $\underline{v}$ satisfies (1.12), that is:

(i) $\underline{v} = \underline{0}$ along Γ_D

(ii) $\underline{v}$ produces finite (normalised) strain energy in the sense that the norm:

$$||\underline{v}||_V = \left(\int_\Omega v_{\alpha,\beta}\, v_{\alpha,\beta}\, dx\right)^{\frac{1}{2}} \qquad \ldots. [1.16]$$

is finite where $dx = dx_1\, dx_2\, dx_3$

K = subset of V consisting of all admissible displacements $\underline{v}$ in V for which $\underline{v}.\underline{n} \leq s$ at all points on the contact surface Γ_C.

$a(\underline{u},\underline{v})$ = virtual work produced by the action of stresses $\sigma_{\alpha\beta}(\underline{u})$ on strains caused by the displacements $\underline{v}$.

$$= \int_\Omega E_{\alpha\beta\gamma\partial}\, u_{\gamma,\partial}\, v_{\alpha,\beta}\, dx$$

$$= \int_\Omega \sigma_{\alpha\beta}(\underline{u})\, \varepsilon_{\alpha\beta}(\underline{v})\, dx$$

where $\varepsilon_{\alpha\beta}(\underline{v})$ is the strain tensor, $\varepsilon_{\alpha\beta}(\underline{v}) = \frac{1}{2}(v_{\alpha,\beta}+v_{\beta,\alpha})$.

$j_{\rho,\varepsilon}(\underline{u},\underline{v})$ = the virtual work of the frictional forces on the displacement $\underline{v}$

$$= \int_{\Gamma_C} \nu\, S_\rho(\sigma_n(\underline{u}))\, \psi_\varepsilon\, (|\underline{v}_t|)ds$$

Where ds is an element of surface area, on Γ_C and ψ_ε is the primitive of ϕ_ε : $\phi_\varepsilon = \psi_\varepsilon'$

$f(\underline{v})$ = virtual work done by the external forces on the displacement $\underline{v}$.

$$= \int_{\Omega} \underline{f}.\underline{v}\,dx + \int_{\Gamma_F} \underline{t}.\underline{v}\,ds$$

With the notation established the variational inequality for the boundary value problem may now be stated.
The solution $\underline{u}$ of the problem defined by (1.10) - (1.15) satisfies

$$a(\underline{u},\underline{v}-\underline{u}) + j_{\rho,\varepsilon}(\underline{u},\underline{v}) - j_{\rho,\varepsilon}(\underline{u},\underline{u}) \geq f(\underline{v}-\underline{u}) \quad \ldots.[1.17]$$

for all admissable displacements $\underline{v}$ in K. [1]

The following proposition was proved by Oden and Pires [1]

Proposition: Let $\underline{u}$ be a sufficiently smooth solution of the Signorini problem with nonlocal nonlinear friction (1.10-1.15). Then $\underline{u}$ is also a solution of the variational inequality (1.17). Conversely, if $\underline{u}$ is a solution of (1.17), then $\underline{u}$ also satisfies the system (1.10-1.15).

If the tangential stress is prescribed, equal to τ say, along Γ_C, it is independent of the displacement $\underline{u}$ and the variational inequality becomes

$$a(\underline{u},\underline{v}-\underline{u}) + j_{o\varepsilon}(\underline{v}) - j_{o\varepsilon}(\underline{u}) \geq f(\underline{u}-\underline{v}) \quad \ldots.[1.18]$$

for all $\underline{v}$ in K.

where $$j_{o\varepsilon} = \int_{\Gamma_C} \tau\psi_{\varepsilon}(|\underline{v}_t|)\,ds \quad \ldots.[1.19]$$

The expression (1.18) can be shown to be equivalent to the constrined minimisation problem of finding $\underline{u}$ in K such that

$$I_\varepsilon(\underline{u}) \leq I_\varepsilon(\underline{v}) \qquad \ldots.[1.20]$$

for all $\underline{v}$ in K where the energy functional I_ε is defined by

$$I_\varepsilon(\underline{v}) = \tfrac{1}{2}a(\underline{v},\underline{v}) - f(\underline{v}) + j_{o\varepsilon}(\underline{v}) \qquad \ldots.[1.21]$$

The minimising function in turn may be shown to satisfy the variational equality (principle of virtual work).

$$a(\underline{u},\underline{v}) + (Dj_{o\varepsilon}, \underline{v}) = f(\underline{v}) \qquad \ldots.[1.22]$$

$$\text{where } Dj_{o\varepsilon}(\underline{u}).\underline{v} = \int_{\Gamma_C} \tau\phi_\varepsilon(|\underline{u}_t|).\frac{\underline{u}_t\cdot\underline{v}_t}{|\underline{u}_t|}\,ds \qquad \ldots.[1.23]$$

see reference [1]

In practice the solution of (1.18) is awkward to implement; instead, the formulation (1.22) is used, the prescribed tangential surface traction being obtained from a previous itteration in the solution procedure. This is made clear in the next two chapters where the finite element approximation of (1.22) is formulated and the solution algorithm is explained.

CHAPTER TWO

THE FINITE ELEMENT APPROXIMATION TO THE VARIATIONAL PROBLEM

The basic idea of the finite element method is to take a body Ω , as in Figure (1.5) of Chapter One, and divide the region Ω into a number of elements Ω^e such that

$$\Omega^e \cap \Omega^f = 0 \quad , \quad \bigcup_{e=1}^{N} \Omega^e = \Omega \qquad \ldots\ldots [2.1]$$

(see Figure 2.1)

The variables of interest are approximated on element Ω^e by defining nodes (see Figure 2.1) and then writing, for any function $\phi(x,y)$,

$$\phi(x,y) = \sum_i \phi^i h_i(x,y) \qquad \ldots\ldots [2.2]$$

where the shape functions $h_i(x,y)$ have the property that

$$\begin{aligned} h_i(x_j,y_j) &= 1 \quad , \quad i=j, \\ &= 0 \quad , \quad i\neq j, \end{aligned} \qquad \ldots\ldots [2.3]$$

(x_j,y_j) being the co-ordinates of node j shown on Figure (2.1).

Hence ϕ^i in (2.2) can be expressed as

$$\phi^i \equiv \phi(x_i,y_i)$$

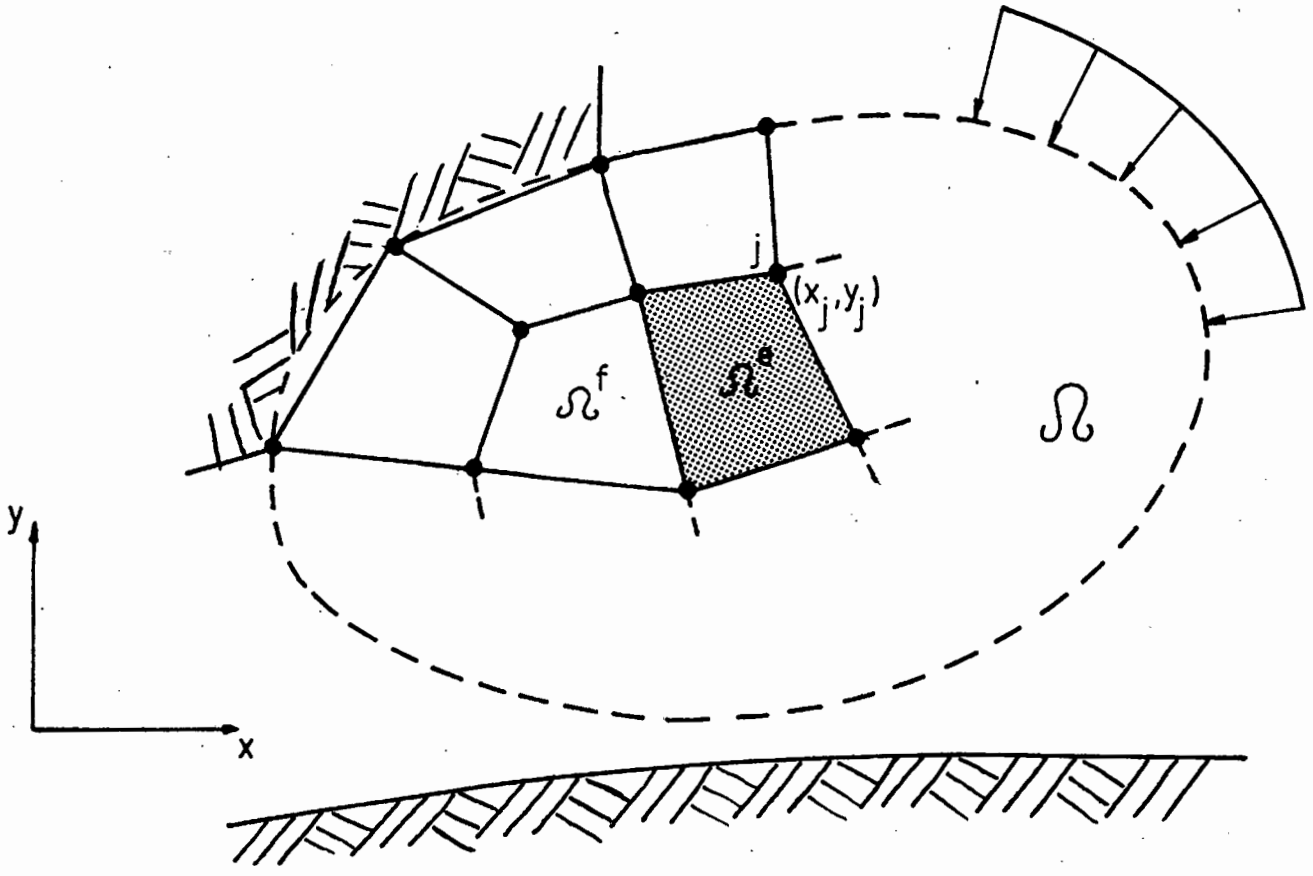

Figure 2.1 The elastic body Ω is divided into elements Ω^e defined by nodes (x_j, y_j). (The midside nodes are left out for clarity).

2.1 The Formulation of the Master Element $\hat{\Omega}$

It is clear that the calculation of element stiffness matrices and load vectors for a curvilinear element Ω^e, such as that indicated in Figure (2.1), would be awkward if performed directly in terms of the x and y co-ordinates shown. The character of the calculations would also change from element to element in the mesh. If we introduce an invertible transformation between a master element $\hat{\Omega}$ of simple shape and an arbitrary element Ω^e, it should be possible to transform the operations of Ω^e so that they hold on $\hat{\Omega}$. This enables the calculations to be performed on the master element. This transformation is done using a simple co-ordinate transformation or mapping of points from $\hat{\Omega}$ onto points in each element.

The master element $\hat{\Omega}$ is defined in natural co-ordinates ξ and η and occupies a region $-1 \leq \xi \leq 1$ and $-1 \leq \eta \leq 1$. (see Figure 2.2).

The map T_e of $\hat{\Omega}$ onto Ω^e is defined by

$$T_e : \quad x = \hat{x}(\xi,\eta) \quad , \qquad y = \hat{y}(\xi,\eta) \quad . \qquad \ldots.[2.4]$$

All vertical and horizontal lines ξ = constant and η = constant on $\hat{\Omega}$ correspond to the curvilinear co-ordinate lines ξ = constant and η = constant in the x-y plane as shown in Figure (2.3). This idea can be extended to incorporate all the elements Ω^e

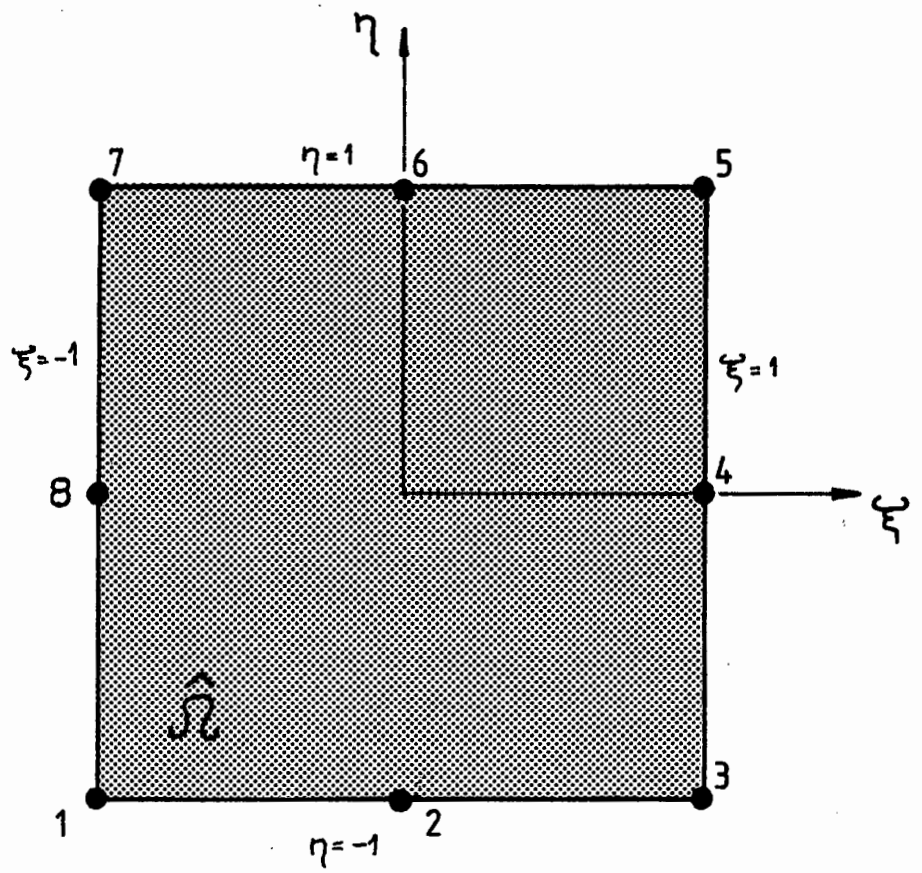

Figure 2.2 The master element $\hat{\Omega}$ defined in natural co-ordinates ξ and η

by setting up maps T_e from $\hat{\Omega}$ to each element Ω^e.

The differentials $d\xi$ and $d\eta$ are related to dx and dy by

$$dx = \frac{\partial x}{\partial \xi} d\xi + \frac{\partial x}{\partial \eta} d\eta \quad ,$$

$$dy = \frac{\partial y}{\partial \xi} d\xi + \frac{\partial y}{\partial \eta} d\eta \quad ,$$

which can be written in matrix form as

$$\begin{bmatrix} dx \\ dy \end{bmatrix} = \begin{bmatrix} \frac{\partial x}{\partial \xi} & \frac{\partial x}{\partial \eta} \\ \frac{\partial y}{\partial \xi} & \frac{\partial y}{\partial \eta} \end{bmatrix} \begin{bmatrix} d\xi \\ d\eta \end{bmatrix} \quad .... [2.5]$$

where the 2x2 matrix of partial derivatives in (2.5) is the Jacobian matrix of the transformation and is denoted by J.

The inverse of (2.5) is also true, that is,

$$\begin{bmatrix} d\xi \\ d\eta \end{bmatrix} = J^{-1} \begin{bmatrix} dx \\ dy \end{bmatrix} \quad .... [2.6]$$

provided that $\det J \neq 0$.

It follows that we may define the inverse map T_e^{-1} which maps Ω^e onto $\hat{\Omega}$, and, which is defined by

$$T_e^{-1} : \quad \xi = \hat{\xi}(x,y) \quad ,$$
$$\eta = \hat{\eta}(x,y) \quad . \quad .... [2.7]$$

(See Figure 2.3)

The shape functions h_i defined in (2.3) may be used to construct the map T_e, that is,

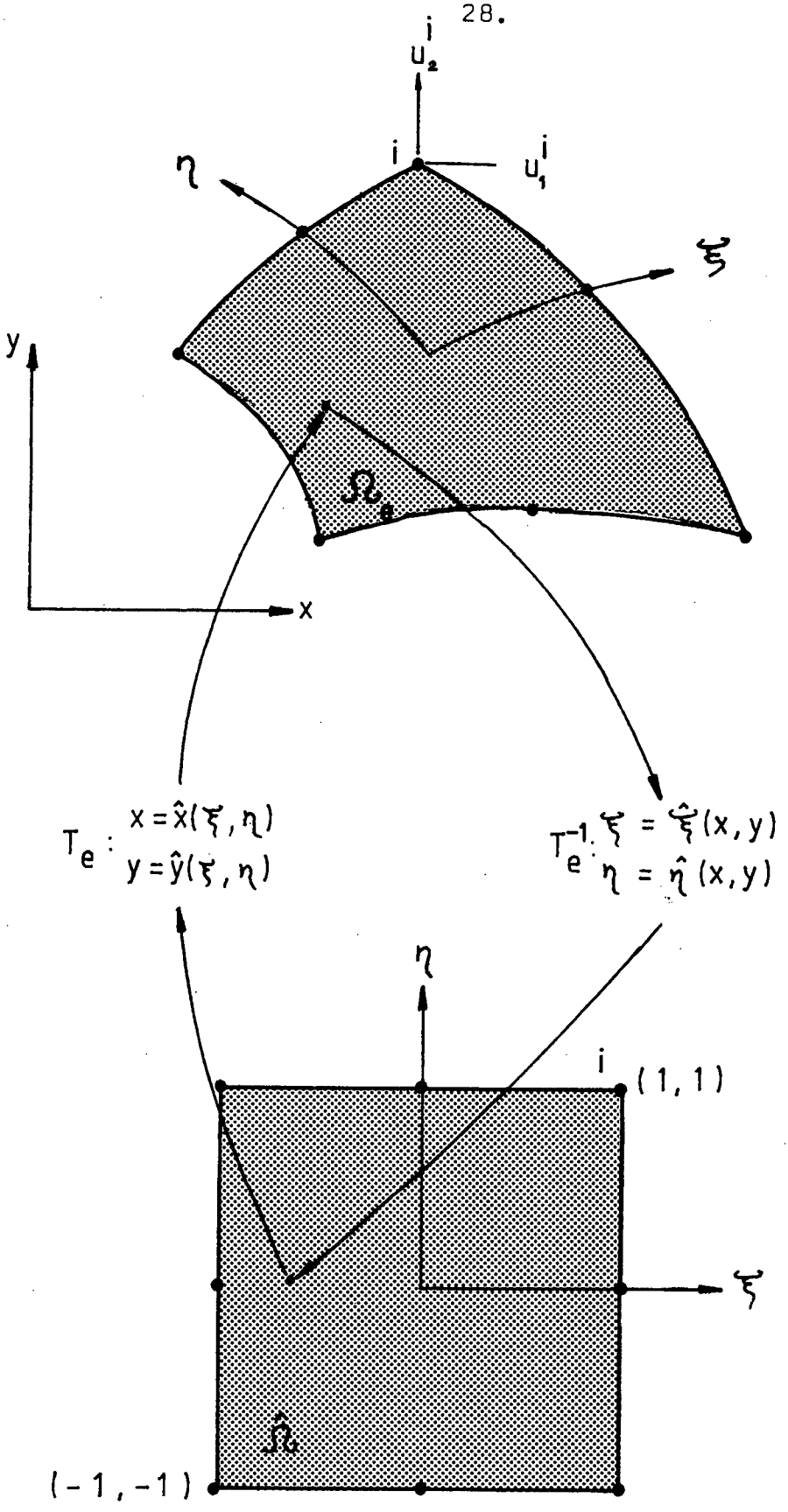

Figure 2.3 The map T_e from the master element $\hat{\Omega}$ to Ω^e and the inverse map T_e^{-1} from Ω^e to $\hat{\Omega}$.

$$T_e : \quad x = \sum_i x_i \hat{h}_i(\xi,\eta) \quad ,$$

$$y = \sum_i y_i \hat{h}_i(\xi,\eta) \quad , \qquad \ldots.[2.8]$$

where the shape functions $\hat{h}_i$ are defined for

the 8-noded master element $\hat{\Omega}$ in Figure (2.2) , by:

for the corner nodes (i = 1,3,5 or 7)

$$\hat{h}_i(\xi_i,\eta_i) = \frac{1}{4}(1 + \xi\xi_i)(1 + \eta\eta_i)(\xi\xi_i + \eta\eta_i - 1)$$

for the midside nodes (i = 2,4,6 or 8)

$$\hat{h}_i(\xi_i,\eta_i) = \frac{\xi_i^2}{2}(1 + \xi\xi_i)(1 - \eta^2) + \frac{\eta_i^2}{2}(1 + \eta\eta_i)(1 - \xi^2) \quad \ldots.[2.9]$$

The images of the shape functions $\hat{h}_i(\xi,\eta)$ in the x-y plane are

$$\hat{h}_i(\xi(x,y),\ \eta(x,y)) = h_i(x,y) \qquad \ldots.[2.10]$$

Therefore the element shape functions $h_i^e = h_i^e(x,y)$ for Ω^e may be obtained from $\hat{h}_i = \hat{h}_i(\xi,\eta)$ once the map T_e and its inverse are known.

The master element $\hat{\Omega}$ used to define the body Ω in the finite element approximation of the variational equality (1.22) was the 8-noded isoparametric element. This element has shape functions defined in (2.9). The displacements at any point in this element are interpolated by

$$u_\alpha(x,y) = \sum_i u_\alpha^i h_i(x,y) \qquad \alpha=1,2 \qquad \ldots.[2.11]$$

where u_α^i is the value of u_α at node i. (See Figure 2.3)

2.2. The Finite Element Approximation to the Variational Principle

From (1.22) in Chapter One we have

$$a(u,v) + (D j_{o\varepsilon}, v) = f(v) \qquad \forall v \in K \qquad \ldots\ [2.12]$$

which for a specific element e is,

$$a(u,v)^e + (D j_{o\varepsilon}, v)^e = f(v)^e \qquad \ldots\ [2.13]$$

Equation (2.13) may be summed over all elements to obtain an approximation of (2.12), that is,

$$\sum_e a(u,v)^e + \sum_e (D j_{o\varepsilon}, v)^e = \sum_e f(v)^e \qquad \ldots\ [2.14]$$

The above expression is the finite element approximation to the variational equality (2.12).

Consider the expression

$$a(u,v)^e = \int_{\Omega^e} E_{\alpha\beta\gamma\partial}\, v_{\alpha,\beta}\, u_{\gamma,\partial}\ dxdy \qquad \ldots\ [2.15]$$

the functions v_α are given by

$$v_\alpha(x,y) = \sum_i v_\alpha^i\, h_i(x,y) \qquad \alpha=1,2$$

so that

$$v_{\alpha,\beta}(x,y) = \sum_i v_\alpha^i \frac{\partial h_i}{\partial x_\beta}(x,y)\ , \qquad \ldots\ [2.16]$$

with a similar result for u_α.

Substituting (2.16) into (2.15) results in

$$a(u,v)^e = \sum_i \sum_j \int_{\Omega^e} E_{\alpha\beta\gamma\partial}\, v_\alpha^i\, u_\gamma^j\, \frac{\partial h_i}{\partial x_\beta}\, \frac{\partial h_j}{\partial x_\partial}\, dx_1 dx_2$$

$$= \sum_i v_\alpha^i \left[\sum_j \int_{\Omega^e} E_{\alpha\beta\gamma\partial}\, h_{i,\beta}\, h_{j,\partial}\, dx_1 dx_2 \right] u_\gamma^j$$

$$= \sum_i \sum_j v_\alpha^i\, k_{\alpha\gamma}^{ij}\, u_\gamma^j \qquad \ldots\ [2.17]$$

where $$k_{\alpha\gamma}^{ij} = \int_{\Omega^e} E_{\alpha\beta\gamma\partial}\, h_{i,\beta}\, h_{j,\partial}\, dx_1 dx_2 \qquad \ldots\ [2.18]$$

The expression (2.17) can be rearranged as

$$a(u,v)^e = \{v\}^T [k]\ \{u\} \qquad \ldots\ [2.19]$$

where $\{v\}^T = (v_1^1, v_2^1, v_1^2, v_2^2, \ldots\ldots v_1^n, v_2^n)$

and $\{u\}^T = (u_1^1, u_2^1, u_1^2, u_2^2, \ldots\ldots u_1^n, u_2^n)$

where n is the number of nodes in the element and the entries of the matrix $[k]$ have the form

$$[k] = \begin{bmatrix} k_{11}^{11} & k_{12}^{11} & k_{11}^{12} & k_{12}^{12} & \cdots & k_{11}^{1n} & k_{12}^{1n} \\ k_{21}^{11} & k_{22}^{11} & k_{21}^{12} & \cdots & \cdots & \cdots & k_{22}^{1n} \\ \cdots & \cdots & \cdots & \cdots & \cdots & \cdots & \cdots \\ k_{21}^{n1} & k_{22}^{n1} & \cdots & \cdots & \cdots & k_{21}^{nn} & k_{22}^{nn} \end{bmatrix}$$

Next consider the term $f(v)^e$:

$$f(v)^e = \int_{\partial\Omega^e} f_\alpha \, v_\alpha \, ds$$

$$= \sum_i \int_{\partial\Omega^e} f_\alpha \, v_\alpha^i \, h_i(x,y) \, ds$$

$$= \sum_i v_\alpha^i \, F_\alpha^i \qquad \ldots\ldots [2.20]$$

where $F_\alpha^i = \int_{\partial\Omega^e} f_\alpha \, h_i(x,y) \, ds$

The expression (2.20) can be written as,

$$f(v)^e = \{v\}^T \{F\} \qquad \ldots\ldots [2.21]$$

where $\{F\}$ is a vector whose entries are F_α^i , that is

$$\{F\}^T = (F_1^1, F_2^1, F_1^2, F_2^2, \ldots\ldots, F_1^n, F_2^n)$$

The frictional term $(Dj_{o\varepsilon}, v)^e$ can be reduced in a similar manner. We have

$$(Dj_{o\varepsilon}, v)^e = \int_{\partial\Omega^e} \tau \, \phi_\varepsilon(|\underline{u}_t|) \, v_\alpha \, t_\alpha \, ds$$

$$= \sum_i \int_{\partial\Omega^e} \tau \, \phi_\varepsilon(|\underline{u}_t|) \, t_\alpha \, v_\alpha^i \, h_i(s) \, ds$$

$$= \sum_i v_\alpha^i \int_{\partial\Omega^e} \tau \, \phi_\varepsilon(|\underline{u}_t|) \, t_\alpha \, h_i(s) \, ds$$

$$= \sum_i v_\alpha^i \, \hat{F}_\alpha^i \qquad \ldots\ldots [2.22]$$

where $h_i(s) = h_i(x(s), y(s))$

and where, in the numerical process, the k-th iterate $\tau^{(k)}$ is found from

$$\tau^{(k)}(s) = \nu \int_{\partial\Omega^e} \omega_\rho(s,t) \, \sigma_n^{(k-1)}(t) \, dt$$

Therefore (2.22) can be written as

$$(Dj_{o\varepsilon}, v) = \{v\}^T \{\hat{F}\} \qquad \ldots\ [2.23]$$

where $\{\hat{F}\}^T = (\hat{F}_1^1, \hat{F}_2^1, \hat{F}_1^2 \ \ldots\ldots \ \hat{F}_1^n, \hat{F}_2^n)$

and $$\hat{F}_\alpha^i = \int_{\partial\Omega^e} \tau\ \phi_\varepsilon(|\underline{u}_t|)\ t_\alpha\ h_i(s)\ ds$$

$$= \int_{\partial\Omega^e} \hat{f}_\alpha\ h_i(s)\ ds$$

where $\hat{f}_\alpha = \tau\ \phi_\varepsilon(|\underline{u}_t|)\ t_\alpha$

Therefore (2.13) can be rewritten as

$$\{v\}^T [k] \{u\} + \{v\}^T \{\hat{F}\} = \{v\}^T \{F\}$$

Since $\{v\}$ is arbitrary the equation

$$[k]\{u\} + \{\hat{F}\} = \{F\} \qquad \ldots\ [2.24]$$

must hold. The entries in $[k]$, $\{F\}$ and $\{\hat{F}\}$ are integrals over volumes or surface areas. For the isoparametric element a gaussian numerical integration technique is used to evaluate the integrals. We discuss this next.

2.3. Gaussian Numerical Integration

The general principle for any function $f(x,y)$ is that for the numerical integration of the expression

$$\int_{\Omega^e} f(x,y)\ dxdy$$

the domain of integration used is the domain $\hat{\Omega}$ in the ξ-η plane. A change of co-ordinates results

in

$$\int_{\Omega^e} f(x,y)\, dxdy = \int_{\hat{\Omega}} f(x(\xi,\eta),y(\xi,\eta))\, detJ\, d\xi d\eta \qquad \ldots\ [2.25]$$

This can then be integrated numerically using gaussian quadrature, that is ,

$$\int_{\Omega^e} f(x,y)\, dxdy \simeq \sum_{A}^{N_f} \sum_{B}^{N_f} f(x(\xi_A,\eta_B),y(\xi_A,\eta_B))\, detJ\, w_A\, w_B \quad \ldots\ [2.26]$$

where (ξ_A,η_A) are the co-ordinates and w_A is the weight factor for gauss point A. The order of integration is specified by N_f. Figure (2.4) shows the position of the gauss points and gives the weight factor values for the gauss points for 2x2 and 3x3 gaussian integration.

Applying this to the terms in (2.24) results in

$$k^{ij}_{\alpha\gamma} = \int_{\Omega^e} E_{\alpha\beta\gamma\partial}\, h_{i,\beta}\, h_{j,\partial}\, dx_1 dx_2$$

$$\simeq E_{\alpha\beta\gamma\partial} \sum_{A}^{N_f} \sum_{B}^{N_f} \hat{h}_{i,\beta}(\xi_A,\eta_B)\, \hat{h}_{j,\partial}(\xi_A,\eta_B)\, detJ\, w_A\, w_B \qquad \ldots\ [2.27]$$

$$F^{i}_{\alpha} = \int_{\partial\Omega^e} f_\alpha\, h_i\, ds$$

$$\sum_{A}^{N_f} f_\alpha(\xi_A)\, \hat{h}_i(\xi_A)\, detJ\, w_A \qquad \ldots\ [2.28]$$

and

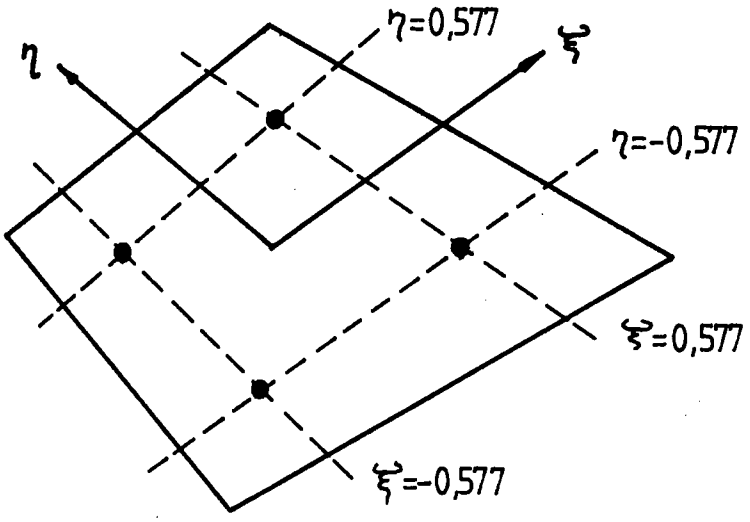

Figure 2.4(a)

The position of the gauss points for 2x2 integration.

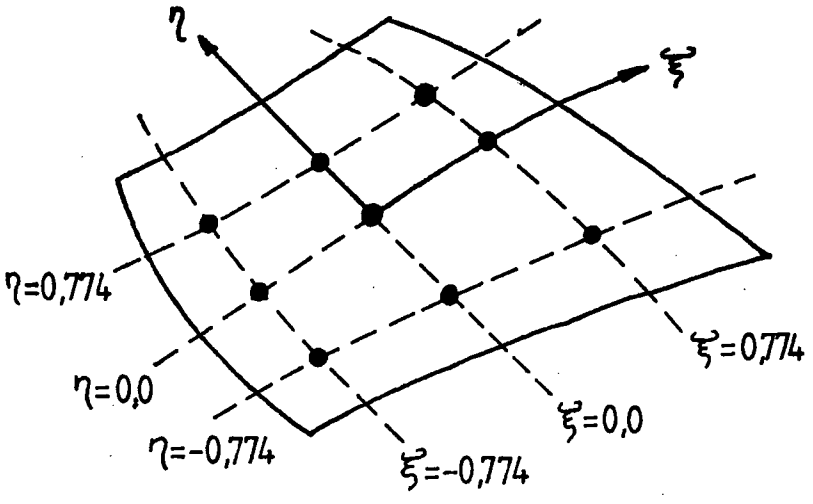

Figure 2.4(b)

The position of the gauss points for 3x3 integration.

Weight factors for Gaussian numeric integration

order of integration	position	weight
2x2	± 0.577	1.00
3x3	± 0.774	0.555̇
	0.000	0.888̇

$$\hat{F}^{i}_{\alpha} = \int_{\partial\Omega^e} \hat{f}_{\alpha}\, h_i \, ds$$

$$= \sum_{A}^{N_f} \hat{f}_{\alpha}(\xi_A)\, \hat{h}_i(\xi_A)\, \det J\, w_A \qquad \ldots\ldots [2.29]$$

Once the integrations have been performed, the equation (2.24) may be solved in an iterative manner (the presence of the term τ in (2.22) necessitates the use of an iterative scheme).

CHAPTER THREE

THE IMPLEMENTATION OF THE FINITE ELEMENT APPROXIMATION

The expression (2.14) in Chapter Two is the finite element approximation to the variational equality developed in Chapter One. The solution of (2.14) requires an iterative algorithm as the tangential stress for the k-th iteration $\hat{f}^{(k)}$ is predicted prior to the calculation of the solution of (2.14). Oden and Pires [3] have proposed an algorithm for the non-classical friction problem which uses a penalty method. The algorithm which is presented here does not use the penalty method.

3.1. The Algorithm for the Nonlocal Nonlinear Friction Law

To start the algorithm we require an initial guess for the region of actual contact: call this region Γ_{C*}, so that the initial guess is $\Gamma_{C*}^{(1)}$ (see Figure 3.1).

On Γ_C we have the unilateral constraint

$$(u_n - s) \leq 0 \quad , \quad \sigma_n \leq 0 \quad ,$$

$$\sigma_n(u_n - s) = 0$$

where s is the initial distance between the boundary and Γ_C, and u_n is the normal displacement at that point on the boundary.

On $\Gamma_{C*}^{(1)}$ we set $u_n^{(1)} - s = 0$ and on $\Gamma_C - \Gamma_{C*}^{(1)}$ we set $\sigma_n^{(1)} = 0$.

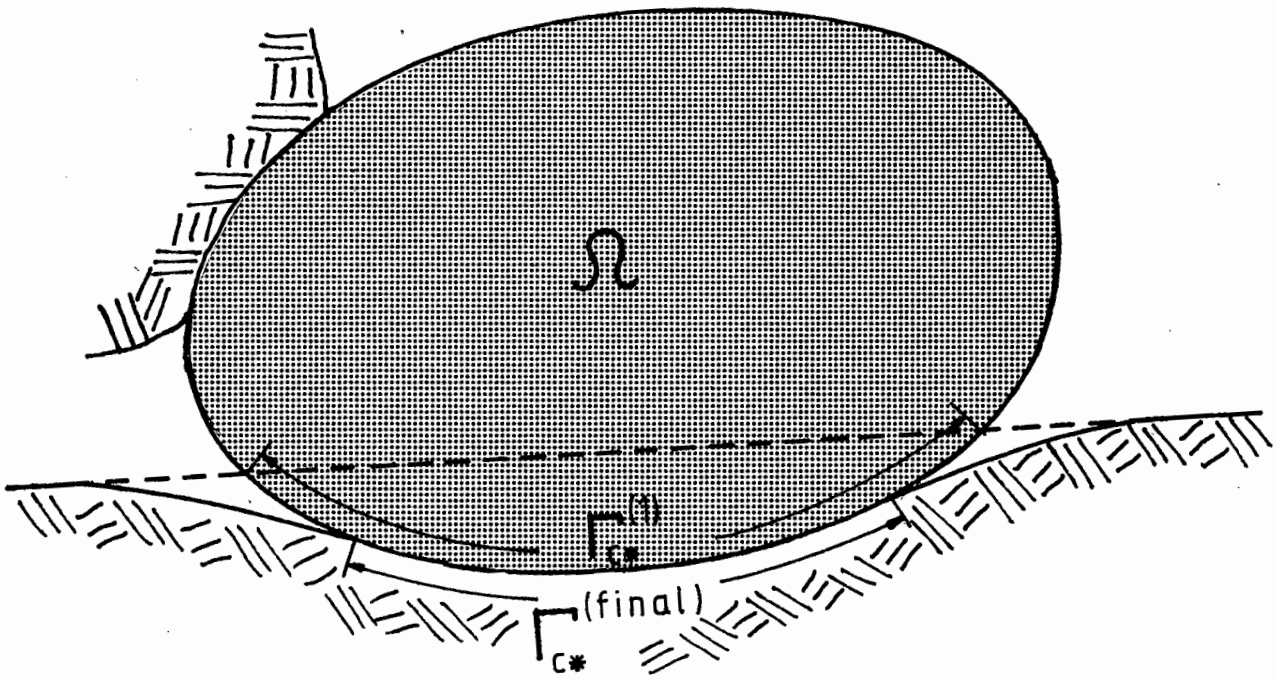

Figure 3.1 The body's final region of contact $\Gamma_{C*}^{(final)}$ compared with the initial guess $\Gamma_{C*}^{(1)}$.

Contact during the first iteration is assumed to be frictionless and so $\hat{f}^{(1)} = 0$. The general procedure is now as follows, for iteration (k) :

Step 1 : Set $\sigma_n^{(k)} = 0$ on $\Gamma_C - \Gamma_{C*}^{(k)}$

and $u_n^{(k)} = s$ on $\Gamma_{C*}^{(k)}$

Calculate the components of the vector $\{\hat{F}\}^{(k)}$ using $\hat{f}^{(k)}$. (This calculation for the first iteration results in $\{\hat{F}\}^{(1)} = 0$ as $\hat{f}^{(1)} = 0$).

Step 2 : Solve $K.u^{(k)} = F - \hat{F}^{(k)}$

Step 3 : Calculate $\sigma_n^{(k)}$ on $\Gamma_{C*}^{(k)}$

and $u_n^{(k)}$ on $\Gamma_C - \Gamma_{C*}^{(k)}$

Step 4 : For each node i in $\Gamma_{C*}^{(k)}$:

if $\sigma_n^{(k)} \leq 0$ then node i remains in $\Gamma_{C*}^{(k+1)}$

if $\sigma_n^{(k)} > 0$ then node i is put into $\Gamma_C - \Gamma_{C*}^{(k+1)}$

For each node i in $\Gamma_C - \Gamma_{C*}^{(k)}$:

if $(u_n^{(k)} - s) < 0$ then node i stays in $\Gamma_C - \Gamma_{C*}^{(k+1)}$

if $(u_n^{(k)} - s) \geq 0$ then node i is put into $\Gamma_{C*}^{(k+1)}$

Step 5 : Set $\hat{f}^{(k+1)} = \nu \int_{\Gamma_C} \omega_\rho \, \sigma_n^{(k)} \, \phi_\varepsilon(|u_t^{(k)}|) \, ds$

along $\Gamma_{C*}^{(k+1)}$

Step 6 : If all the checks in Step 4 are satisfied and $|| \sigma_n^{(k)} - \sigma_n^{(k-1)} || < \varepsilon$ for some tolerance ε and some appropriate norm, then the approximate solution has been found. If not, return to Step 1 with the new $\Gamma_{C*}^{(k+1)}$ and $\hat{f}^{(k+1)}$.

This is the basic algorithm. The methods of calculation of the quantities appearing in this algorithm are now explained.

3.2. The Calculation of $\{\hat{F}\}^{(k)}$

From Chapter Two we have

$$\hat{F}_{\alpha i}^{(k)} = \sum_A \hat{f}_\alpha^{(k)}(\xi_A)\, h_i(\xi_A)\, \det J\, w_A \qquad \ldots\ [3.1]$$

where

$$\hat{f}_\alpha^{(k)}(\xi_A) = \nu \sum_B \omega_\rho(|\xi_A - \xi_B|)\, \sigma_n^{(k-1)}(\xi_B)\, \det J\, w_B\, \phi_\varepsilon^{(k-1)}(\xi_A) \qquad \ldots\ [3.2]$$

and is evaluated in the previous iteration.

There are two possible methods of calculating (3.1) :

(i) if $\hat{f}^{(k)}$ is given at gauss points along the boundary, (3.1) can be calculated directly ; or

(ii) the expression (3.1) may be evaluated along the closest two rows of internal gauss points, these values may then be linearly extrapolated onto the boundary (see Figure 3.2).

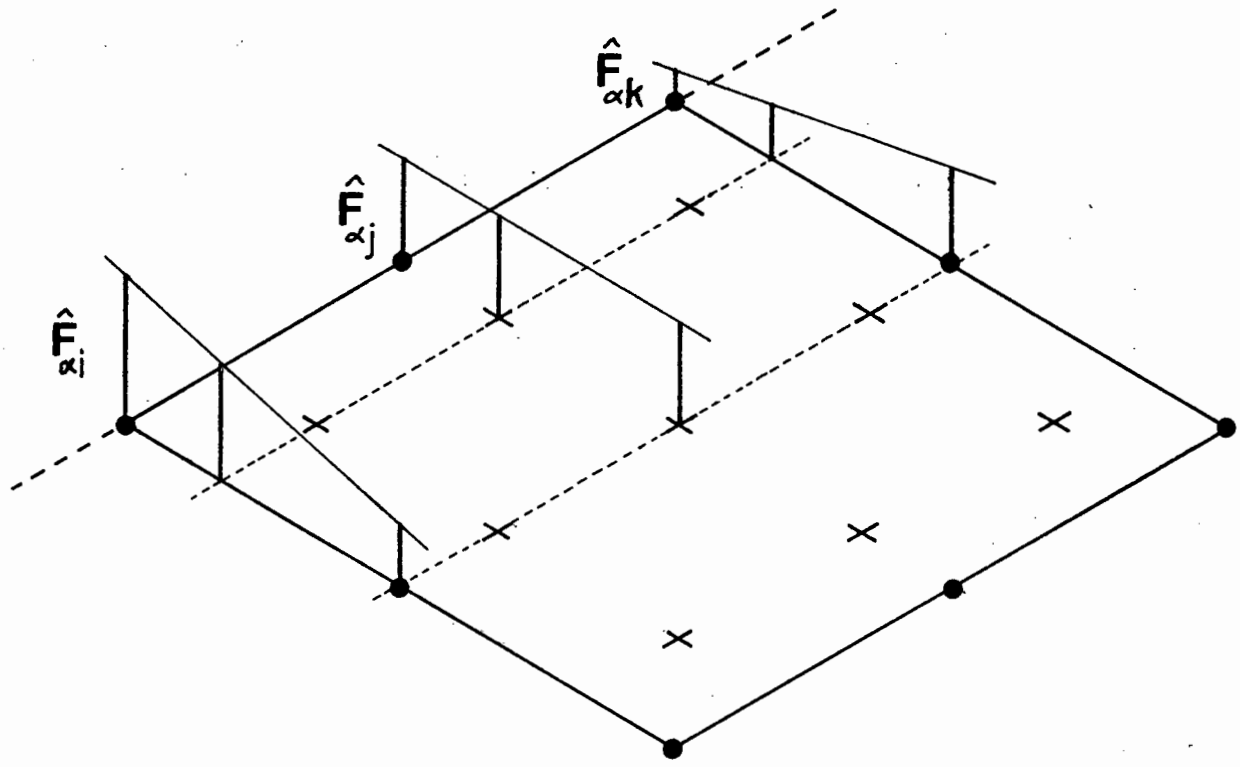

Figure 3.2 The extrapolation of $\hat{F}_{\alpha i}$ onto the boundary nodes using the results of the integral evaluated at the closest two rows of gauss points.

Both of these methods result in $\hat{F}^{(k)}_{\alpha i}$ being evaluated at node i for an element edge.

3.3. The Calculation of σ_n and u_n along Γ_C

The unit vectors tangent $(\underline{t})$ and normal $(\underline{n})$ to the frictional edge and the map $\det J^e$ are required for the calculation of the normal stress (σ_n) and normal displacement (u_n) at any point on the element boundary.

3.3.1. Calculation of $\underline{t}$, $\underline{n}$ and $\det J^e$

The boundary edges are assumed to be linear. Therefore calculation of $\underline{t}$, $\underline{n}$ and $\det J^e$ is straight forward. Consider the element shown in Figure (3.3) with co-ordinates along the frictional edge of (x_i, y_i) and (x_k, y_k) . The length of the edge is :

$$\ell^e = ((x_k - x_i)^2 + (y_k - y_i)^2)^{\frac{1}{2}} \qquad \ldots\ldots [3.3]$$

Therefore $\underline{t}$ along the frictional edge is

$$\underline{t} = \left[\frac{x_k - x_i}{\ell^e} \; ; \; \frac{y_k - y_i}{\ell^e} \right]$$

$$= (t_1, t_2)$$

The normal vector is calculated by rotating $\underline{t}$ through 90 degrees, that is,

$$\underline{n} = (-t_2, t_1)$$

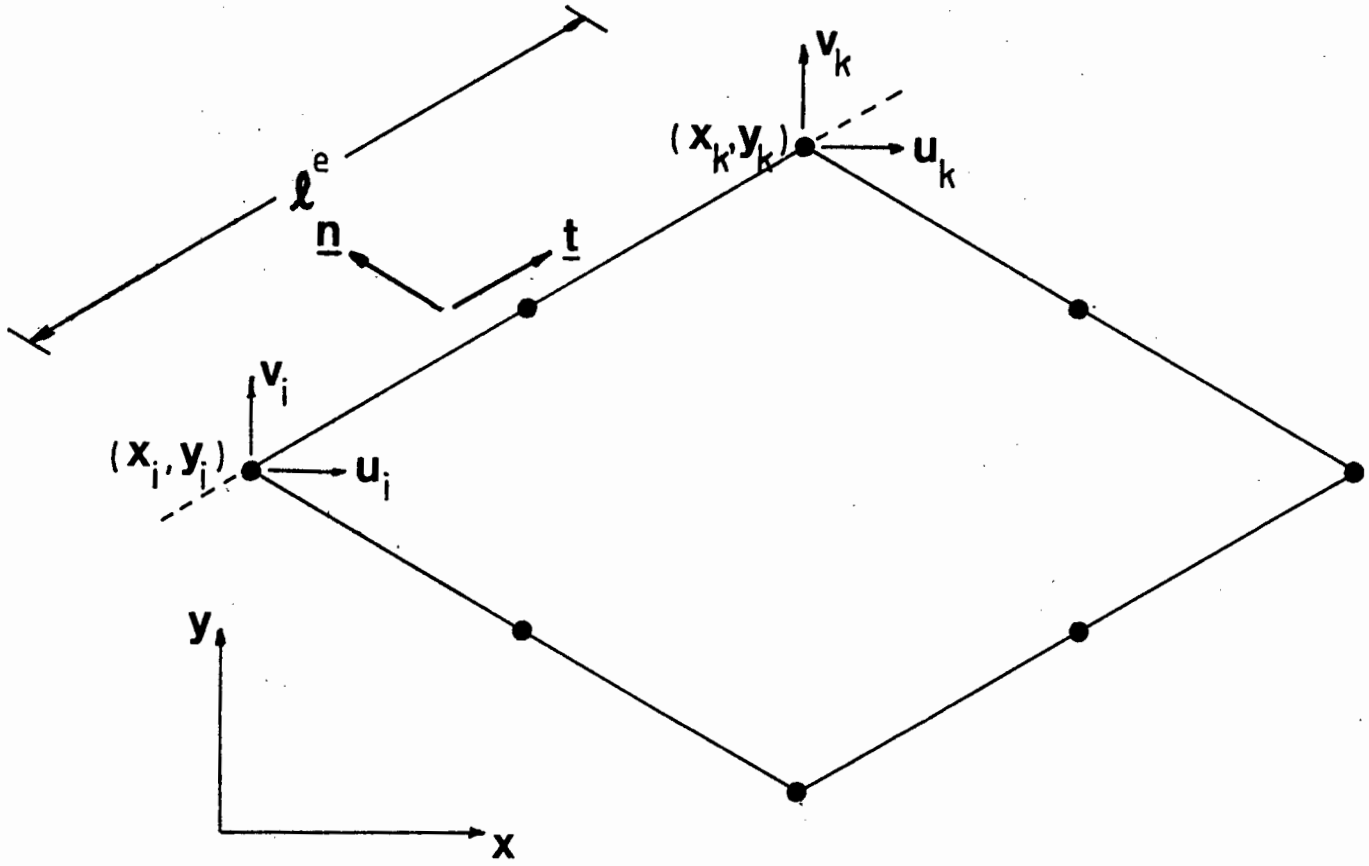

Figure 3.3 A boundary element with the tangential vector $\underline{t}$ and normal vector $\underline{n}$ defined along its frictional edge.

The edges are assumed to remain linear so that the term $\det J^e$ is a ratio of the element lengths. The master element length is 2 (ξ and η range from -1 to +1) and so the mapping factor is

$$\det J^e = \frac{\ell^e}{2} \qquad \ldots\ [3.4]$$

From the solution of $K.u^{(k)} = F - \hat{F}^{(k)}$ the stress tensor $\sigma_{\alpha\beta}$ is evaluated at the internal gauss points and the displacements are given at the nodes. This implies that the calculation of u_n at the nodes involves the calculation of the components of u_α in the direction of the normal vector $\underline{n}$.

The calculation of σ_n at the internal gauss points is

$$\sigma_n = \sigma_{\alpha\beta}\, n_\alpha n_\beta \quad \ldots \quad \alpha=1,2 \qquad \ldots\ [3.5]$$

which in matrix notation is

$$\sigma_n = (n_1, n_2) \cdot \begin{bmatrix} \sigma_{11} & \sigma_{12} \\ \sigma_{12} & \sigma_{22} \end{bmatrix} \begin{bmatrix} n_1 \\ n_2 \end{bmatrix} \qquad \ldots\ [3.6]$$

This calculation is performed at all of the gauss points within an element, resulting in a σ_n value at each gauss point. These values are then extrapolated using linear extrapolation techniques.
The values of σ_n at the two closest rows of gauss points to the boundary, are extrapolated onto the gauss points on the boundary. From there the σ_n values are extrapolated onto the nodes. (See Figures 3.4(a)-(d) for the various types of extrapolation for the different orders of integration).

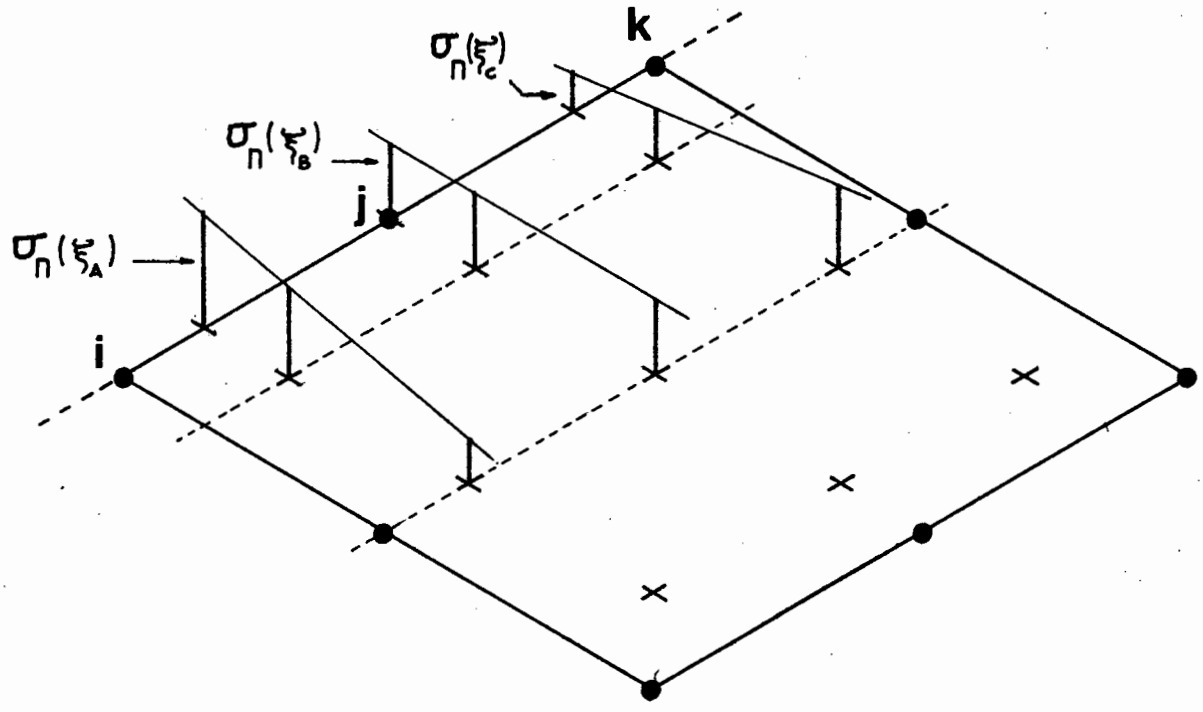

Figures 3.4(a) The extrapolation of σ_n from the internal gauss points onto the boundary gauss points for 3x3 gaussian quadrature.

(b) The extrapolation of σ_n onto the nodes for 3x3 gaussian quadrature.

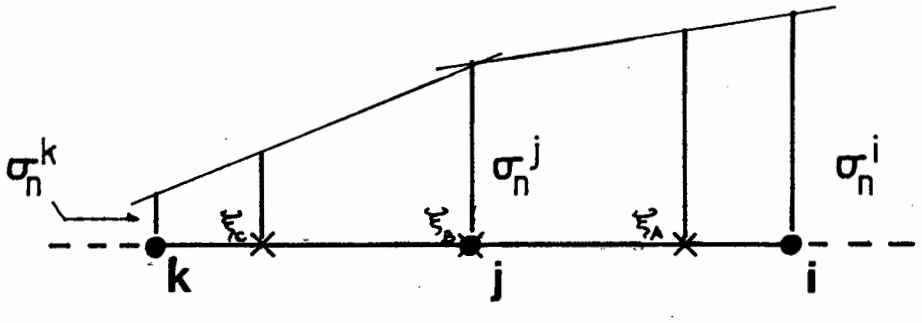

Once these calculations have been carried out and the checks along Γ_c have been performed, the new tangential stress $\hat{f}^{(k+1)}$ can be calculated.

3.4. The Calculation of the new $\hat{f}^{(k+1)}$

The value $\hat{f}^{(k+1)}$ as defined in (3.2) must be evaluated either at the internal gauss points (for use in the second method in Section (3.2)) or along the boundary gauss points (for use in the first method).
Both these evaluations of (3.2) initially require the calculation of σ_n and ϕ_ε at the internal gauss points. The normal stress calculations has been explained in Section (3.3). The calculation of the nonlinear function ϕ_ε at the internal gauss points is shown next.

3.4.1. The Calculation of ϕ_ε at the Internal Gauss Points

The nonlinear function ϕ_ε is a function of the magnitude of the tangential displacement (u_t). Therefore it is necessary to evaluate u_t at the internal gauss points.

The tangential displacement at point (x,y) is

$$u_t(x,y) = u_\alpha(x,y)\, t_\alpha \quad .... \quad \alpha=1,2 \qquad ....[3.7]$$

As previously stated, the values of u_α are given at the nodes of the elements, therefore using (2.11) from Chapter Two, equation (3.7) for any point (x,y)

becomes

$$u_t(x,y) = \sum_i h_i(x,y)\, u_\alpha^i\, t_\alpha \qquad \ldots\ldots [3.8]$$

which in natural co-ordinates is

$$u_t(\xi_A,\eta_A) = \sum_i \hat{h}_i(\xi_A,\eta_A)\, u_\alpha^i\, t_\alpha \qquad \ldots\ldots [3.9]$$

In matrix form (3.9) becomes

$$(u_t) = (Q_A)^T(u) \qquad \ldots\ldots [3.10]$$

where

$$(Q_A)^T = (\hat{h}_1(\xi_A,\eta_A)t_1 \; ; \; \hat{h}_i(\xi_A,\eta_A)t_2 \; ; \; \hat{h}_2(\xi_A,\eta_A)t_1 \; \ldots\ldots \; \hat{h}_n(\xi_A,\eta_A)t_2)$$

and

$$(u)^T = (u_1 \; ; \; v_1 \; ; \; u_2 \; ; \; v_2 \; \ldots\ldots \; u_n \; ; \; v_n)$$

This is for a specific gauss point (ξ_A,η_A). The tangential displacement at all the internal gauss points are thus found from

$$\begin{bmatrix} u_t(\xi_A,\eta_A) \\ u_t(\xi_B,\eta_B) \\ \vdots \\ u_t(\xi_{N_g},\eta_{N_g}) \end{bmatrix} = \begin{bmatrix} (Q(\xi_A,\eta_A))^T \\ (Q(\xi_B,\eta_B))^T \\ \vdots \\ (Q(\xi_{N_g},\eta_{N_g}))^T \end{bmatrix} \begin{bmatrix} u_1 \\ v_1 \\ \vdots \\ u_n \\ v_n \end{bmatrix}$$

or $(u_t) = [Q^*](u)$

where

$$Q^* = \begin{bmatrix} \hat{h}_1(\xi_A,\eta_A)t_1 \; ; \; \hat{h}_1(\xi_A,\eta_A)t_2 \; ; \; \hat{h}_2(\xi_A,\eta_A)t_1 & \dots & \hat{h}_n(\xi_A,\eta_A)t_2 \\ \hat{h}_1(\xi_B,\eta_B)t_1 \; ; & \cdot & \cdot \\ \cdot & \cdot & \cdot \\ \cdot & \cdot & \cdot \\ \hat{h}_1(\xi_{N_g},\eta_{N_g})t_1 \; ; & \cdot & \dots \; \hat{h}_n(\xi_{N_g},\eta_{N_g})t_2 \end{bmatrix}$$

Where n is the number of nodes in the element and

N_g is the number of gauss points in the element.

The nonlinear function ϕ_ε defined in (1.7(a)) or (1.7(b)) in Chapter One is dependent on the tangential displacement. Therefore, if $\underline{u}_t$ is evaluated at the internal gauss points, ϕ_ε may be evaluated there as well. The vector

$$\underline{\phi}_\varepsilon = \begin{bmatrix} \phi_\varepsilon(\xi_A,\eta_A) \\ \phi_\varepsilon(\xi_B,\eta_B) \\ \vdots \\ \phi_\varepsilon(\xi_{N_g},\eta_{N_g}) \end{bmatrix} \qquad \dots.[3.11]$$

is formed where

$$\phi_\varepsilon(\xi_I,\eta_I) = 1 \qquad \text{if } |u_t(\xi_I,\eta_I)| > \varepsilon$$

$$= \frac{|u_t(\xi_I,\eta_I)|}{\varepsilon} \quad \text{if } |u_t(\xi_I,\eta_I)| \leq \varepsilon$$

and ε is the nonlinear parameter defined in Chapter One.

At this point, both σ_n and ϕ_ε are known at the internal gauss points and so the calculation of $\hat{f}^{(k+1)}$ may begin.

The calculation of

$$\hat{f}^{(k+1)}(\xi_A) = \nu \sum_B \omega_\rho(|\xi_A-\xi_B|)\ \sigma_n(\xi_B)\ \det J^e\ w_B\ \phi_\varepsilon(\xi_A)$$

along a line of constant η implies a summation over the gauss points. The nonlocal function ω_ρ is evaluated depending on the gauss point at which $\hat{f}^{(k+1)}$ is being evaluated.

3.4.2. The Nonlocal Function ω_ρ

The function ω_ρ is a bell-shaped function defined by expression (1.2) in Chapter One. When numerically integrating over ω_ρ to calculate $\hat{f}^{(k+1)}(\xi_B)$ the function ω_ρ is centred at gauss point (ξ_B) and extends from $-\rho$ to $+\rho$ in either direction. (See Figure 3.5). There are two problems which are encountered when this is done:

(i) The function ω_ρ may not extend to the next gauss point (see Figure 3.6(a)). This necessitates the introduction of local gauss points onto which σ_n and ϕ_ε are linearly extrapolated (see Figure 3.6(b)), in order to obtain a better estimate of the integral. The integration is then performed over the local gauss points.

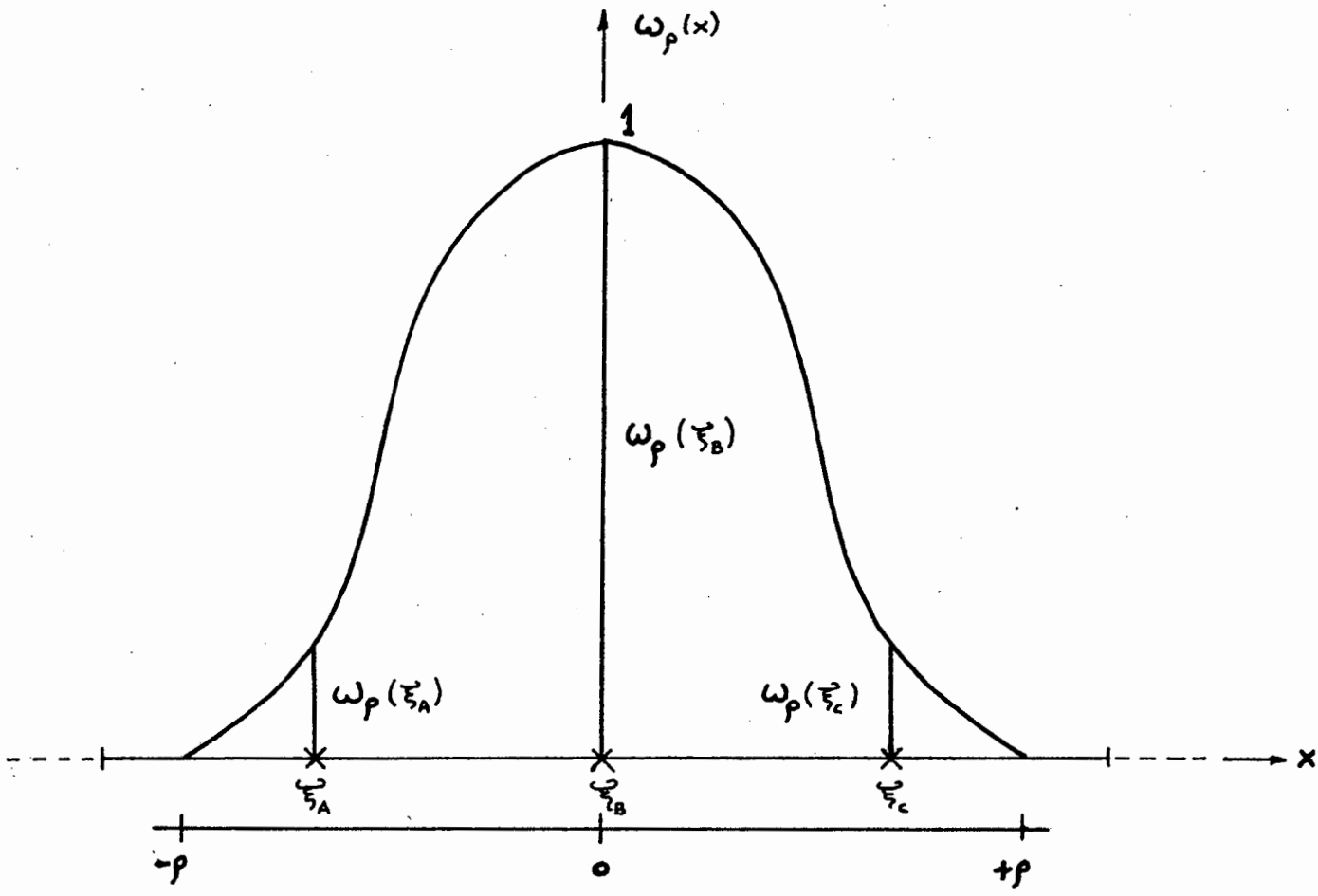

Figure 3.5 The shape of ω_ρ along the line of integration when centred over ξ_B.

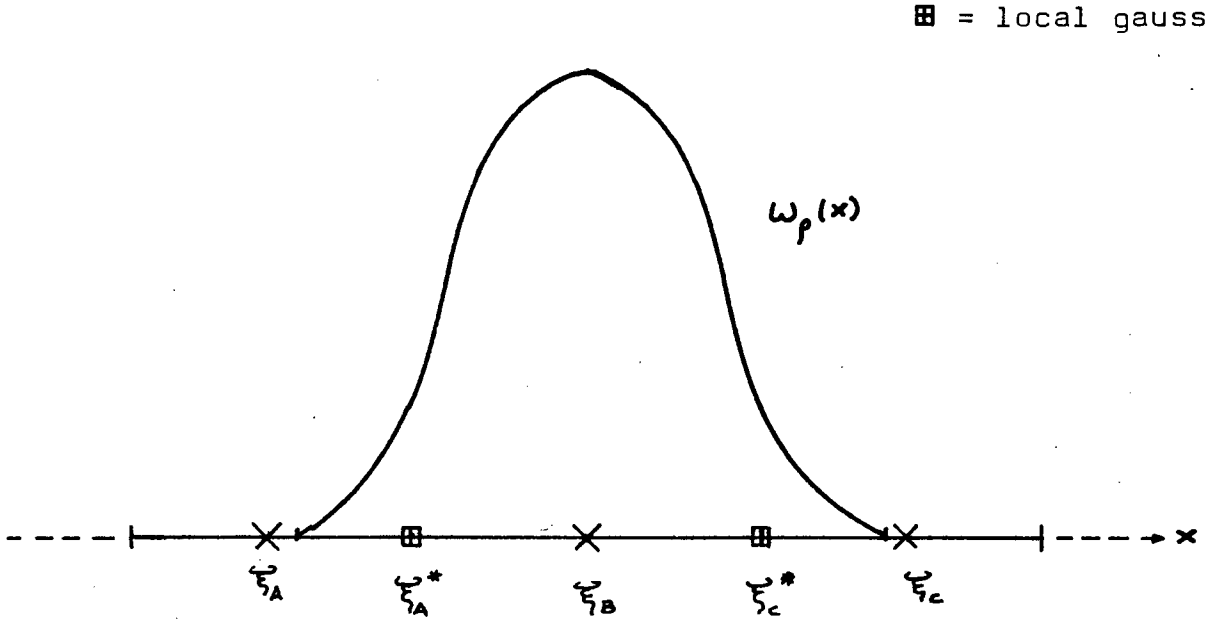

Figures 3.6 (a) The case when ω_ρ does not extend over more than one gauss point.

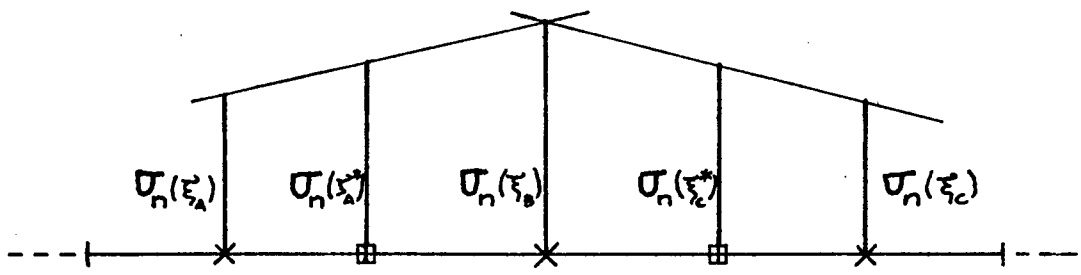

(b) The interpolation of σ_n onto the local gauss points.

(ii) The second problem arises when the ω_ρ function extends into the next element (see Figure 3.7(a)). This problem is solved by assessing whether the ω_ρ functions for the left and right adjacent gauss points extend into the element under consideration. If this is so, then the integration is performed over the section which encroached on the element (see Figure 3.7(b)) and added to the value $\hat{f}^{(k+1)}$ for the adjacent gauss point.

Depending on which method is being used in evaluating $\{\hat{F}\}^{(k)}$, the $\hat{f}^{(k+1)}$ will either be evaluated at the gauss points within the element, or the values of σ_n and ϕ_ε will be extrapolated onto the boundary gauss points and $\hat{f}^{(k+1)}$ will be evaluated on each boundary gauss point. The extrapolation of ϕ_ε onto the boundary is done in the same way as for σ_n (see Figures 3.4(a) and (c)).

3.5. The Convergence Check on σ_n

Once $\Gamma_{C^*}^{(k+1)}$ has been specified, the convergence check on σ_n is performed. This is of the form:

$$R_F = \left[\frac{\sum_i (\sigma_{ni}^L - \sigma_{ni}^P)^2}{\sum_i (\sigma_{ni}^P)^2} \right]^{\frac{1}{2}}$$

where σ_{ni}^L = the latest normal stress at boundary node i, and,

σ_{ni}^P = the previous normal stress at boundary node i.

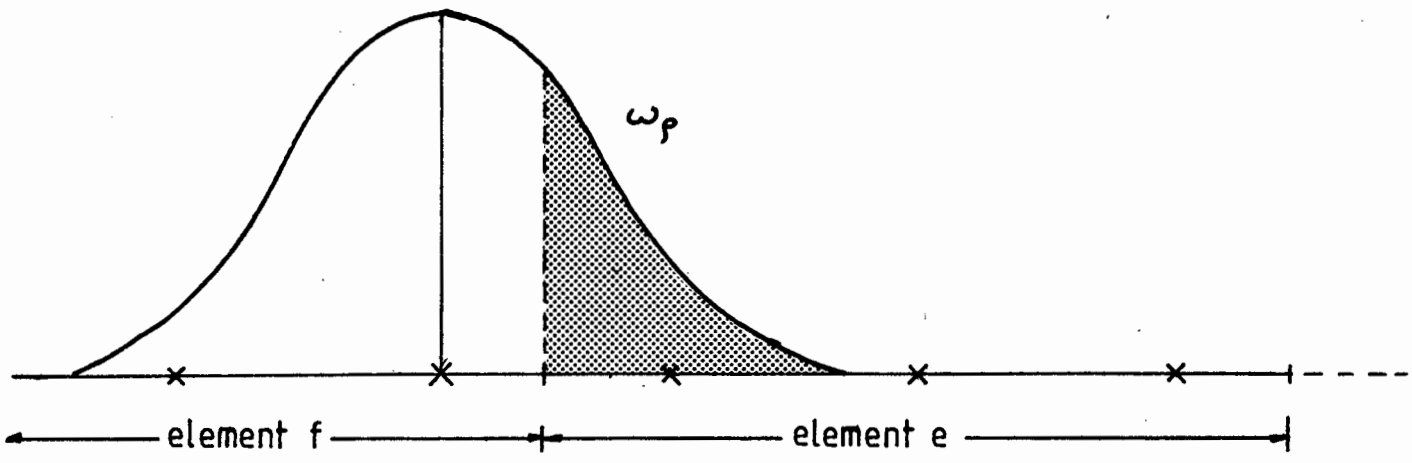

Figures 3.7(a) The case when ω_ρ extends over gauss points in adjacent elements.

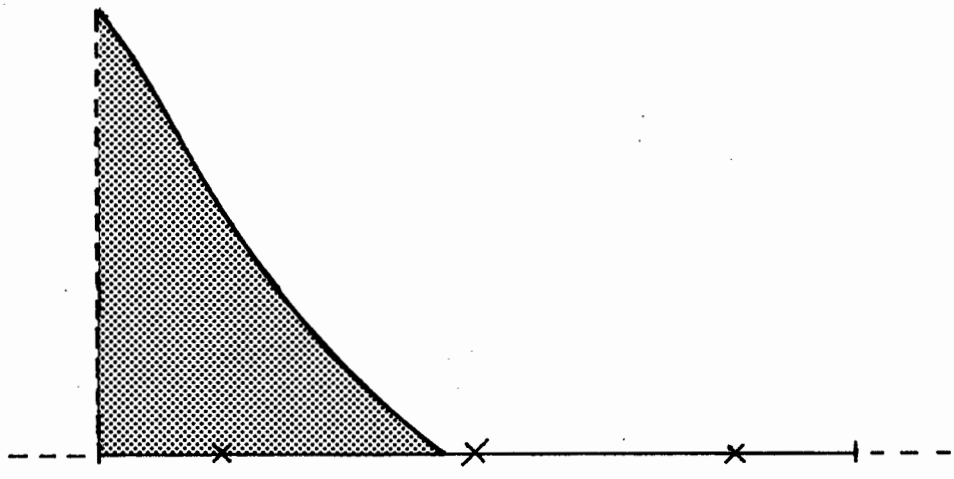

(b) The area which is integrated in element e.

If R_F is within a required tolerance, then the iteration is assumed to have converged; if not, then the algorithm returns to Step 1 with the new values of $\hat{f}^{(k+1)}$ and $\Gamma_{C^*}^{(k+1)}$.

In the next Chapter we discuss a series of problems which have been solved using this algorithm.

CHAPTER FOUR

NUMERICAL EXAMPLES

Five examples are discussed here with a view to illustrating the effects of the friction law; two of these are in plane strain, two are axisymmetric and one is plane stress. These problems were solved using both methods of extrapolation for the calculation of frictional terms; however, the two methods were found to give very similar results and so the results given in this chapter are those found using only one method, namely, the method of extrapolating the integrals. Both methods of extrapolation also proved to be equally stable.

4.1. Plane Strain Examples

(i) The rectangular punch

This problem consists of a rectangular punch of dimensions 1 x 1 units indenting an elastic half-space, whose material properties are Young's modulus $E = 1000$ units and Poisson's ratio of 0.3. The properties of the frictional boundary are:

the coefficient of friction $\nu = 0.3$,

the nonlocal parameter ρ varies between 0.008 and 0.015, and

the nonlinear parameter $\varepsilon = 10^{-4}$

The analysis has been carried out using a similar mesh to that used by Oden and Pires [3] in a similar example. The mesh consists of 56 8-noded isoparametric elements (see Figure 4.1). The displaced shape for an indentation of 0.25 units is shown in Figure 4.2.

The normal and tangential stresses are plotted for a variation in ρ from 0.008 to 0.015 in Figure 4.3, and the closed-form solution given by Green and Zerna [19] for the frictionless problem is also shown. The variable Y is the total normal force acting on the boundary. The numeric solution for the normal stress correlates closely to the theoretical solution, the theoretical solution becoming infinite at the edge of the punch, while the numerical solution remains finite but large.

The main effect of the nonlocal parameter ρ is seen in the vicinity of the edge of the punch; clearly, nonlocalization causes the peak in tangential stress at the edge to be reduced, the reduction increasing with an increase in ρ. In this example, the tangential displacement is due to the elastic deformation of the asperities. There is no gross sliding. This example has also been discussed by Oden and Pires [3]; however, we are unable to compare results as they do not give a value for the indentation in their paper.

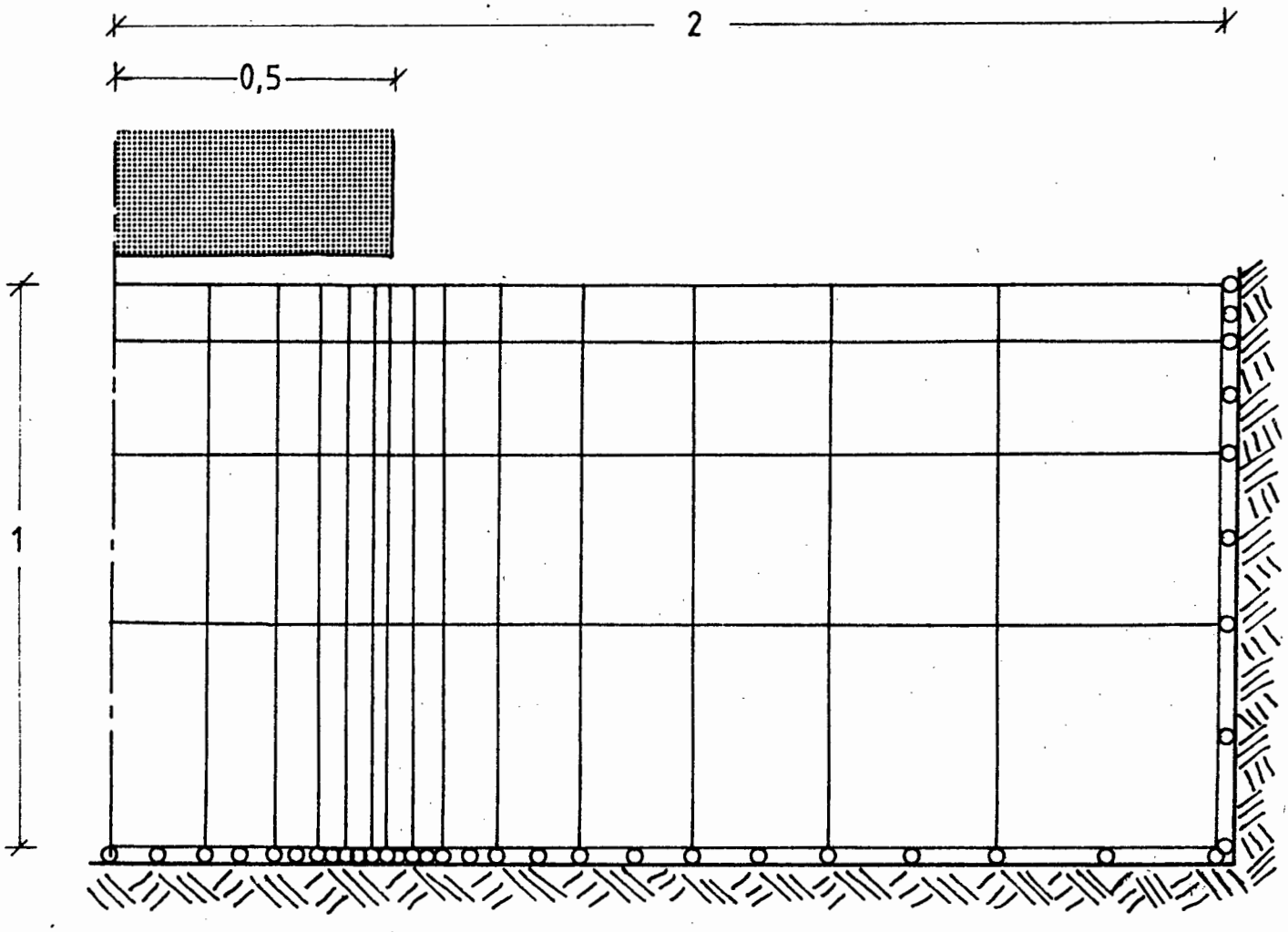

Figure 4.1. The finite element mesh for the indentation of an elastic half-space by a rigid rectangular punch.

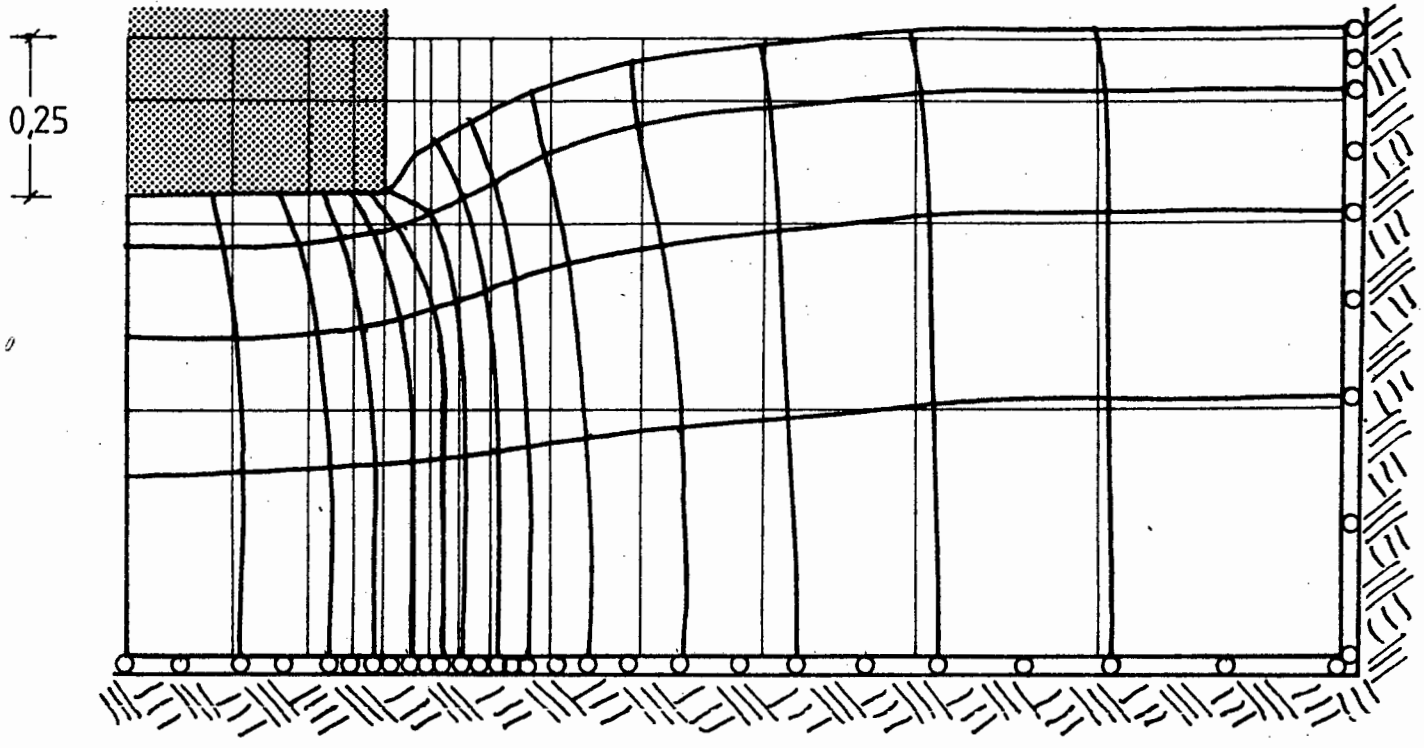

Figure 4.2. The computed deformed configuration for a rigid rectangular punch indenting a half-space by 0.25 units.

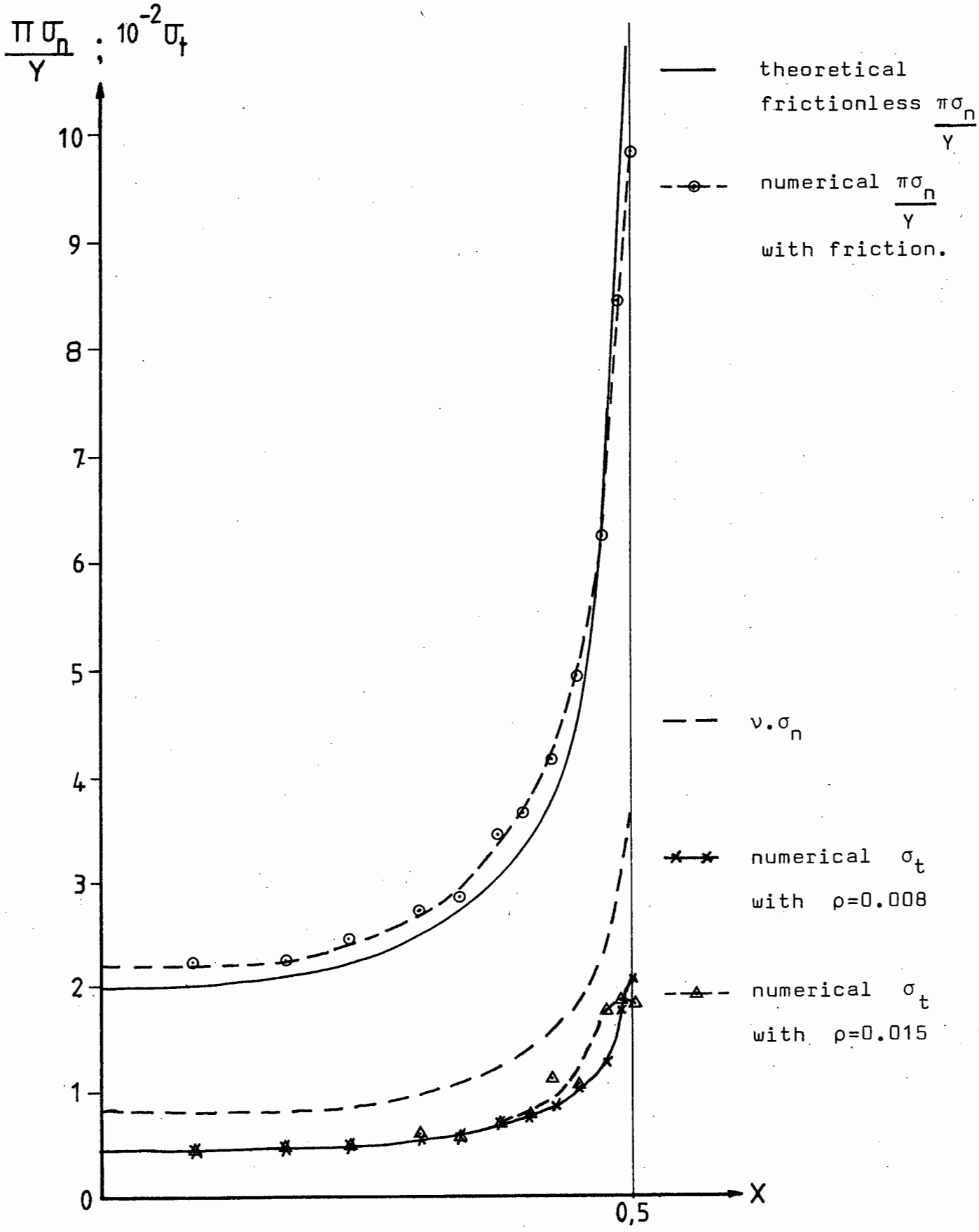

Figure 4.3. Normal and tangential stress profiles (on the contact surface) for the rectangular punch example.

(ii) The cylindrical punch

This problem consists of a rigid cylindrical punch of radius 8 units, its curved surface indenting an elastic half-space. This elastic half-space has a value of $E = 1000$ units and a Poisson's ratio of 0.3. The properties of the frictional boundary on the elastic half-space are :

$$\nu = 0.3 \quad ,$$
$$0.01 \leq \rho \leq 0.05 \ ,$$
$$\varepsilon = 10^{-4} \quad .$$

The finite element mesh used is similar to that used by Campos, Oden and Kikuchi[2] for a similar problem with Coulomb friction. Here, 44 8-noded isoparametric elements are used (see Figure 4.4). The deformed shape for an indentation of 0.48 units is given in Figure 4.5.

The mesh grading and values of ρ chosen for this problem result in the weighting function ω_ρ overlapping two elements when it is centred at one of the gauss points of the elements having length ≤ 0.05 (see Figure 4.4). Recalling from our earlier discussion that the present routine allows only for integration over two elements, we see that a possible source of error is present here. However, this situation is exceptional, and most cases are adequately dealt with by the scheme outlined in Section 3.4.2 of Chapter Three.

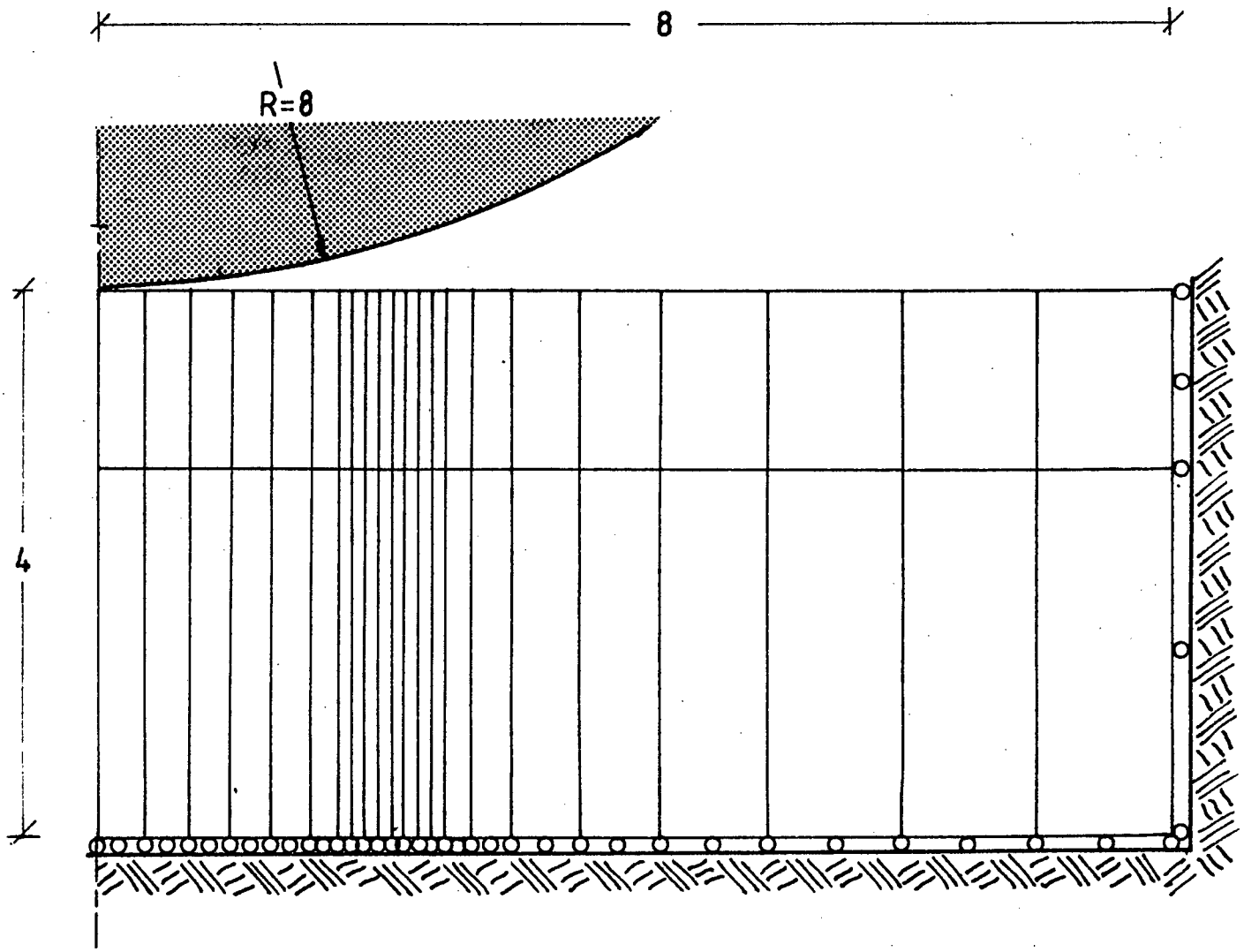

Figure 4.4. The finite element mesh for the indentation of an elastic half-space by a rigid cylindrical punch on its side.

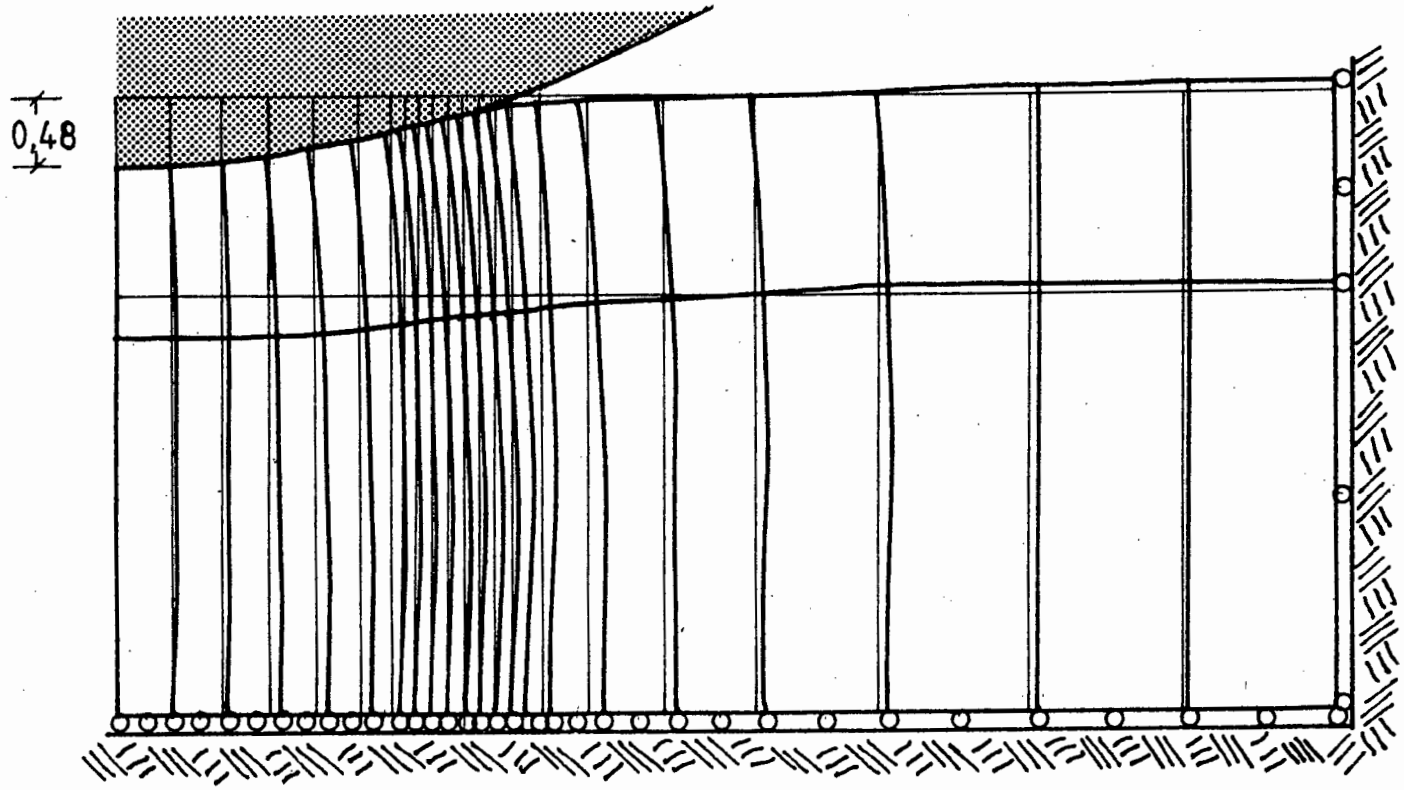

Figure 4.5. The computed deformed configuration for a rigid cylindrical punch on its side indenting a half-space by 0.48 units.

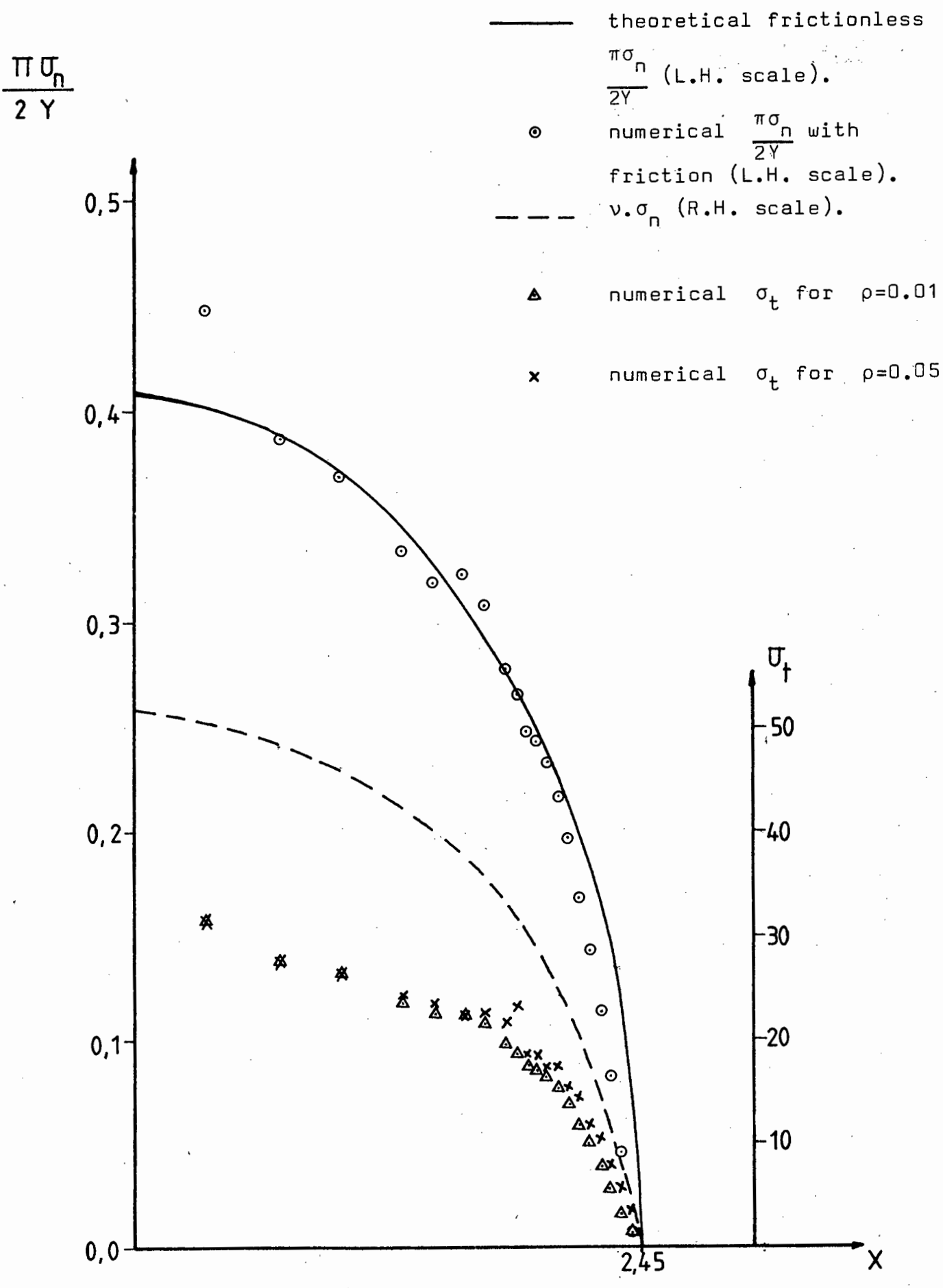

Figure 4.6. Normal and tangential stress profiles on the contact surface, for the example of the cylindrical punch on its side.

In Figure 4.6, the normal stress along the frictional boundary is plotted against the theoretical normal stress calculated using a formulation by Green and Zerna [19] for cylindrical punches assuming that friction is negligible. The variable Y is the total normal force acting over the area which is in contact. The variation between the two values of normal stress is seen to be minimal. The tangential stress is plotted for $\rho=0.01$ and $\rho=0.05$. The nonlocal effect is not as pronounced as in the previous example, presumably since the punch has no sharp edges and so there is, in fact, not as severe a localization of stress at the edges of the contact area.

4.2. Axisymmetric Examples

(i) The flat annular punch

This example consists of a rigid annular punch indenting an elastic half-space. The elastic half-space has a Young's modulus $E = 1000$ units and a Poisson's ratio of 0.3. The properties of the frictional boundary on the elastic body are :

$$\nu = 0.3 \quad ,$$
$$0.02 \leq \rho \leq 0.13 \quad ,$$
$$\varepsilon = 10^{-4} \quad .$$

The finite element mesh used is similar to that used by Campos, Oden and Kikuchi [2] for the Coulomb solution to this problem, and is shown in Figure 4.7. This mesh

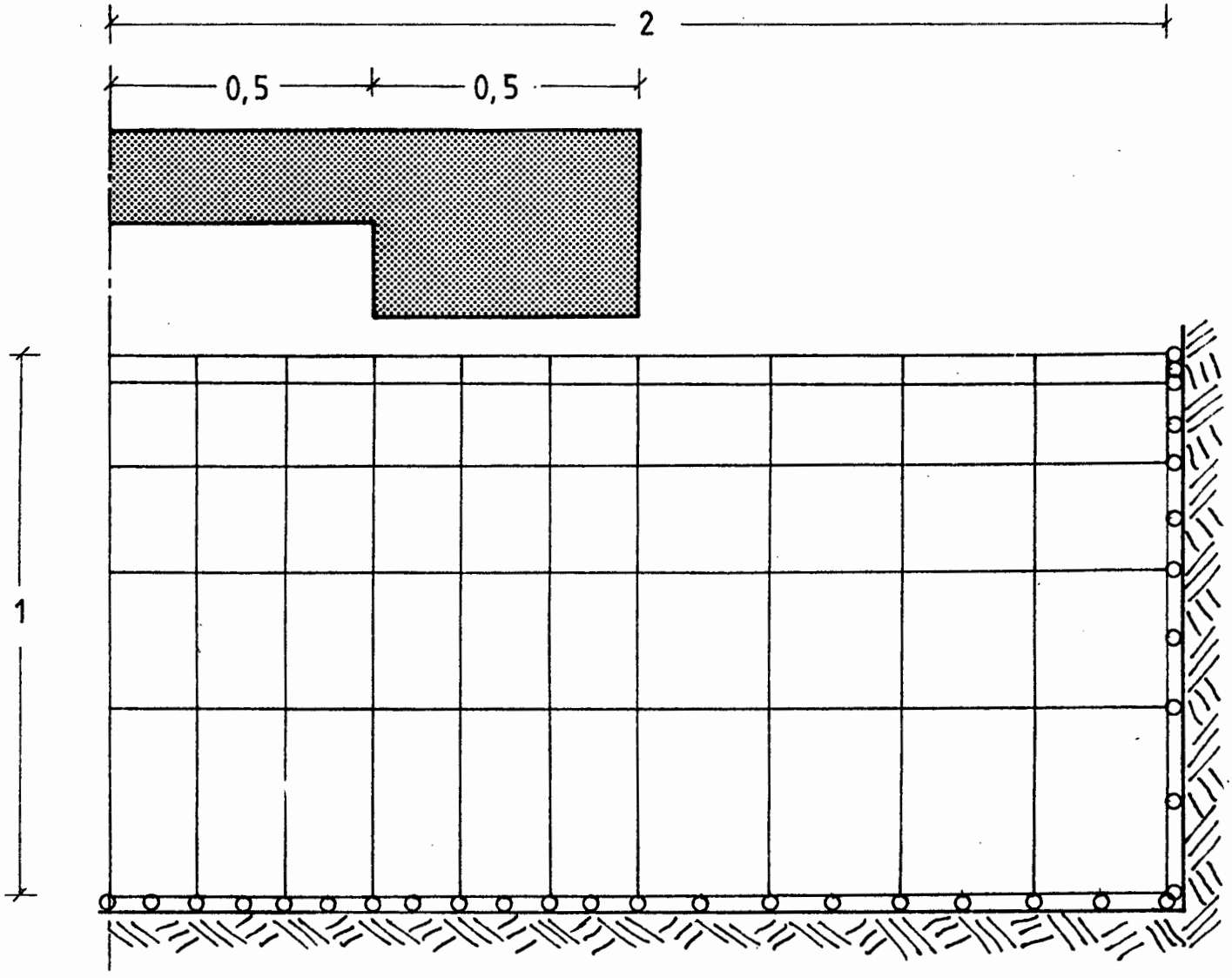

Figure 4.7. The finite element mesh for the indentation of an elastic half-space by an annular punch.

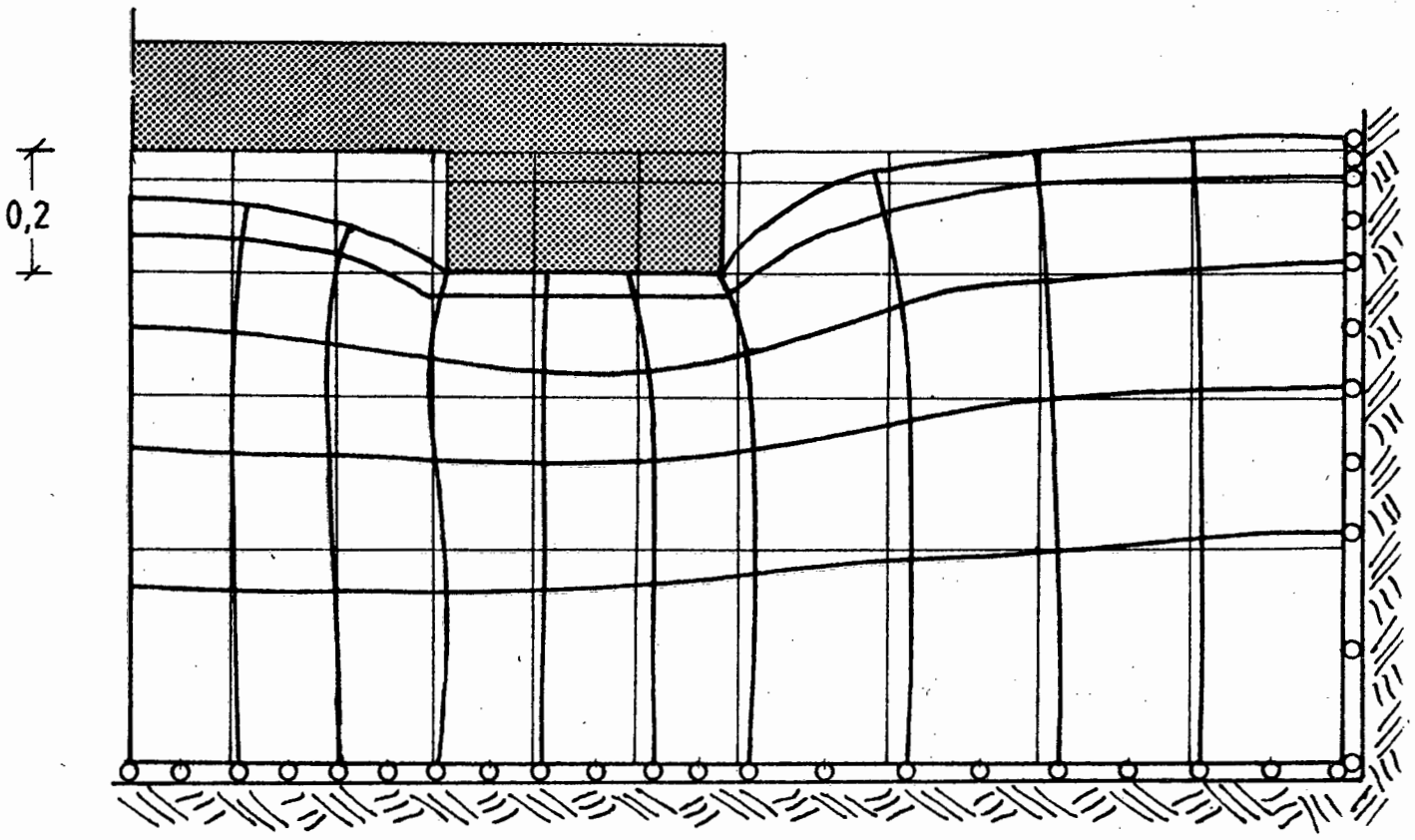

Figure 4.8. The computed deformed configuration for annular punch indenting an elastic half-space by 0.2 units.

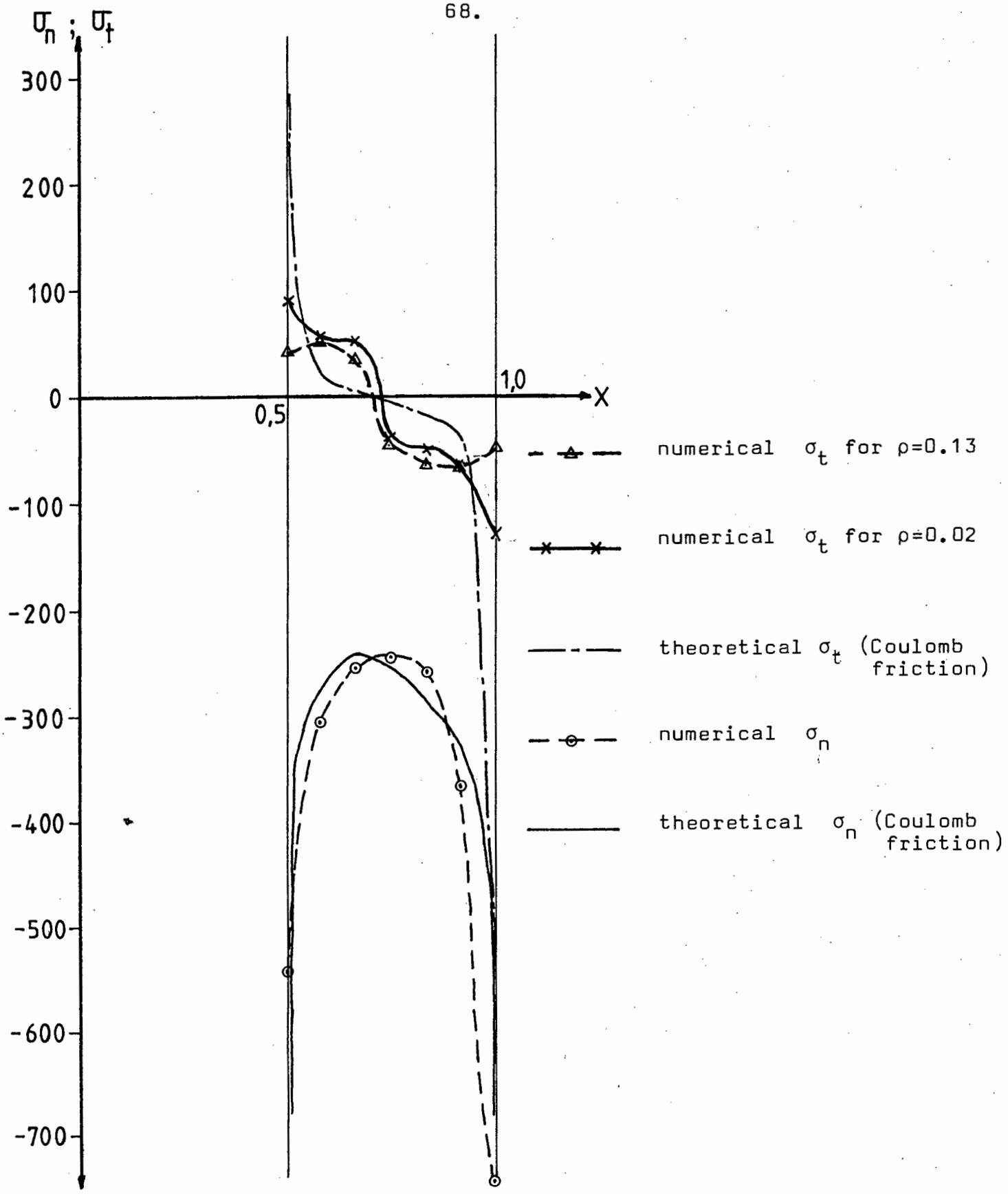

Figure 4.9. Normal and tangential stress profiles on the contact surface for the annular punch.

consists of 50 8-noded axisymmetric isoparametric elements.

The deformed shape for an indentation of 0.2 units is shown in Figure 4.8. Curves of normal stress and tangential stress along the contact area, are shown in Figure 4.9, for different values of ρ.

For the same indentation and different values of ρ, it is seen that as ρ approaches zero, the solution of the tangential stress approaches the Coulomb solution. When ρ is large, the peaks in tangential stress at the punch edges are smoothed out, (see Figure 4.9) as in the first plane strain example.

(ii) The cylindrical punch on its end

This example consists of a rigid cylindrical punch of radius 0.5 units on its end, indenting an elastic half-space. The elastic half-space has Young's modulus $E = 1000$ units and a Poisson's ratio of 0.3. The properties of the frictional boundary on the elastic half-space are :

$$\nu = 0.3 \quad ,$$
$$0.008 \leq \rho \leq 0.015 \quad ,$$
$$\varepsilon = 10^{-4} \quad .$$

The finite element mesh used is similar to that used by the first plane strain example. This mesh consists of 56 8-noded axisymmetric isoparametric finite elements (see Figure 4.10). The deformed shape for an indentation of 0.2 units is given in Figure 4.11.

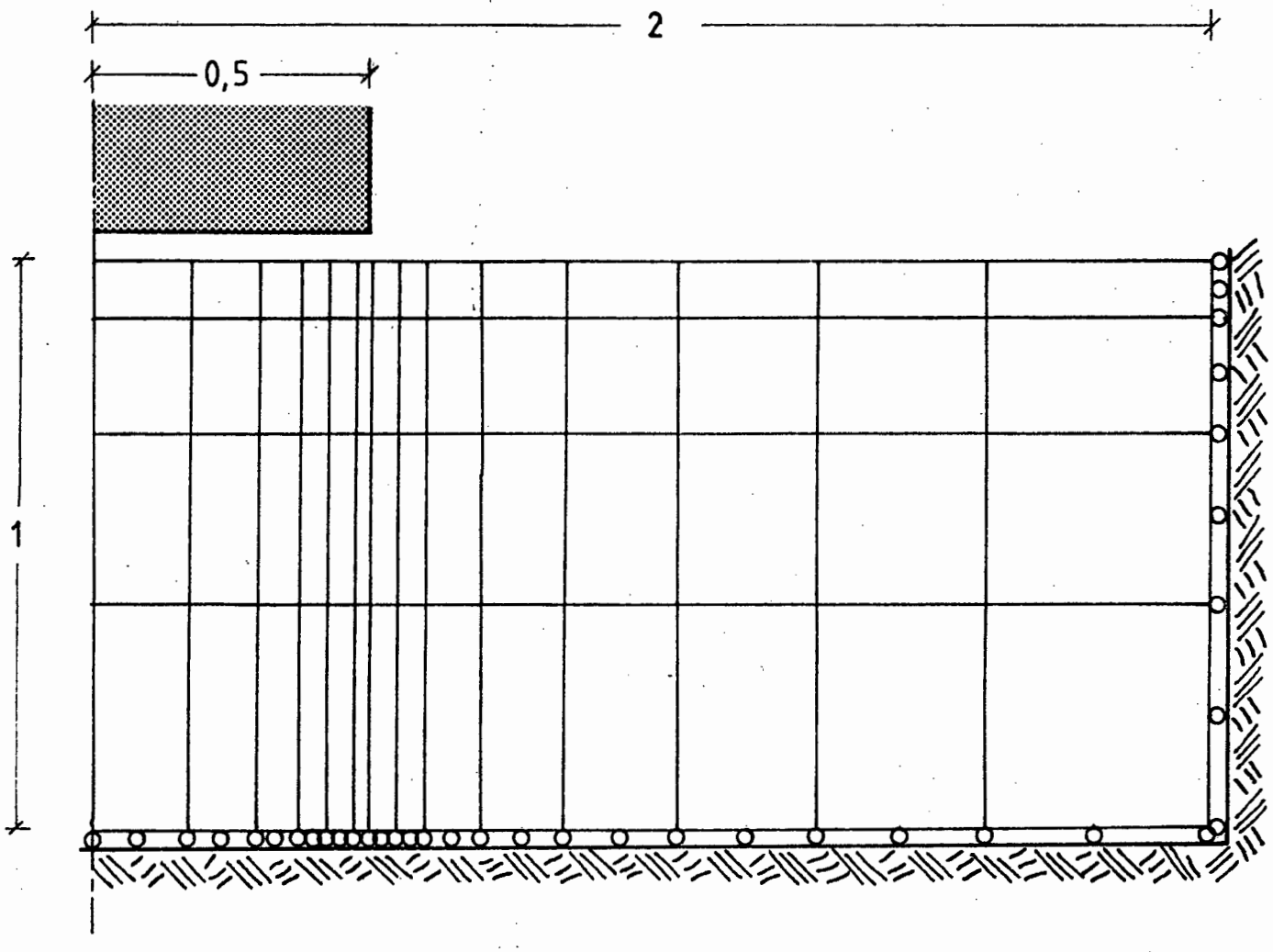

Figure 4.10. The finite element mesh for the indentation of an elastic half-space by the flat side of a rigid cylindrical punch.

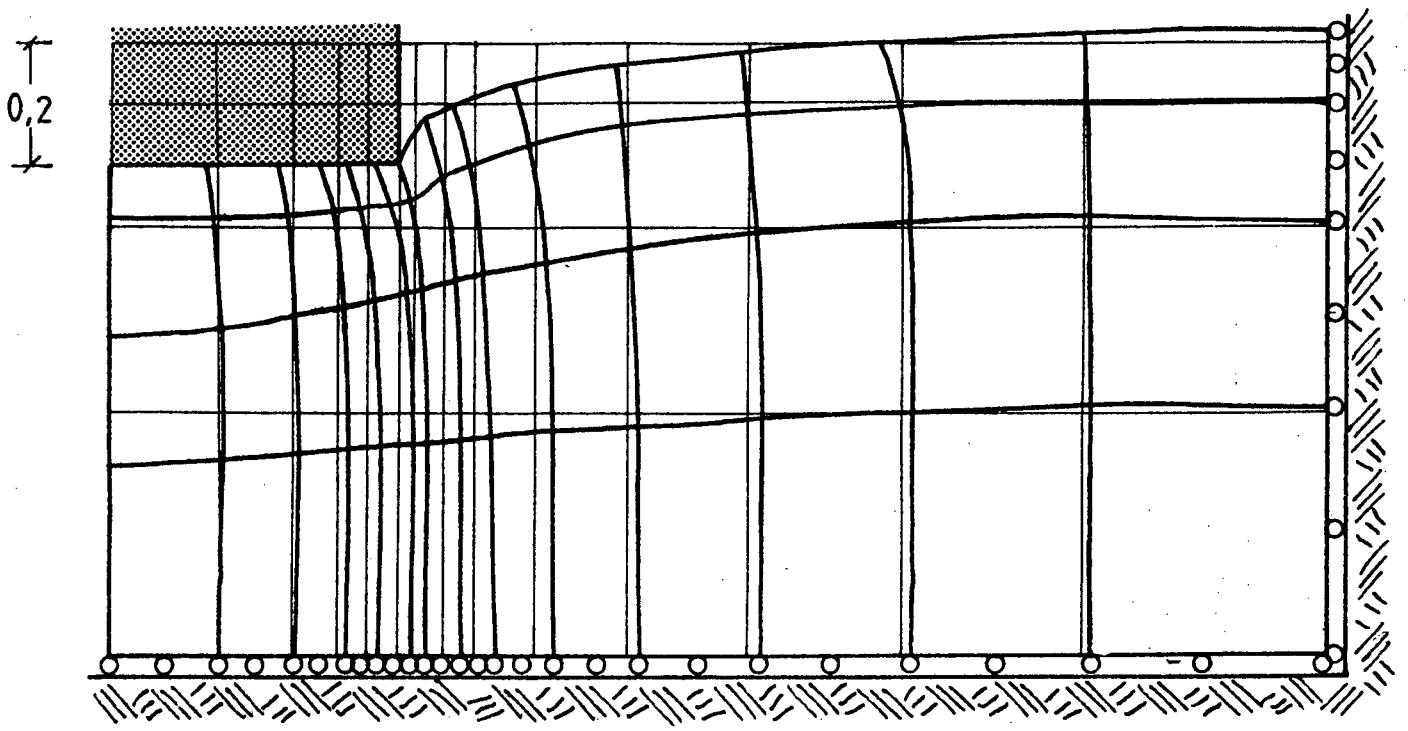

Figure 4.11. The computed deformed configuration for the flat side of a rigid cylinder indenting an elastic half-space by 0.2 units.

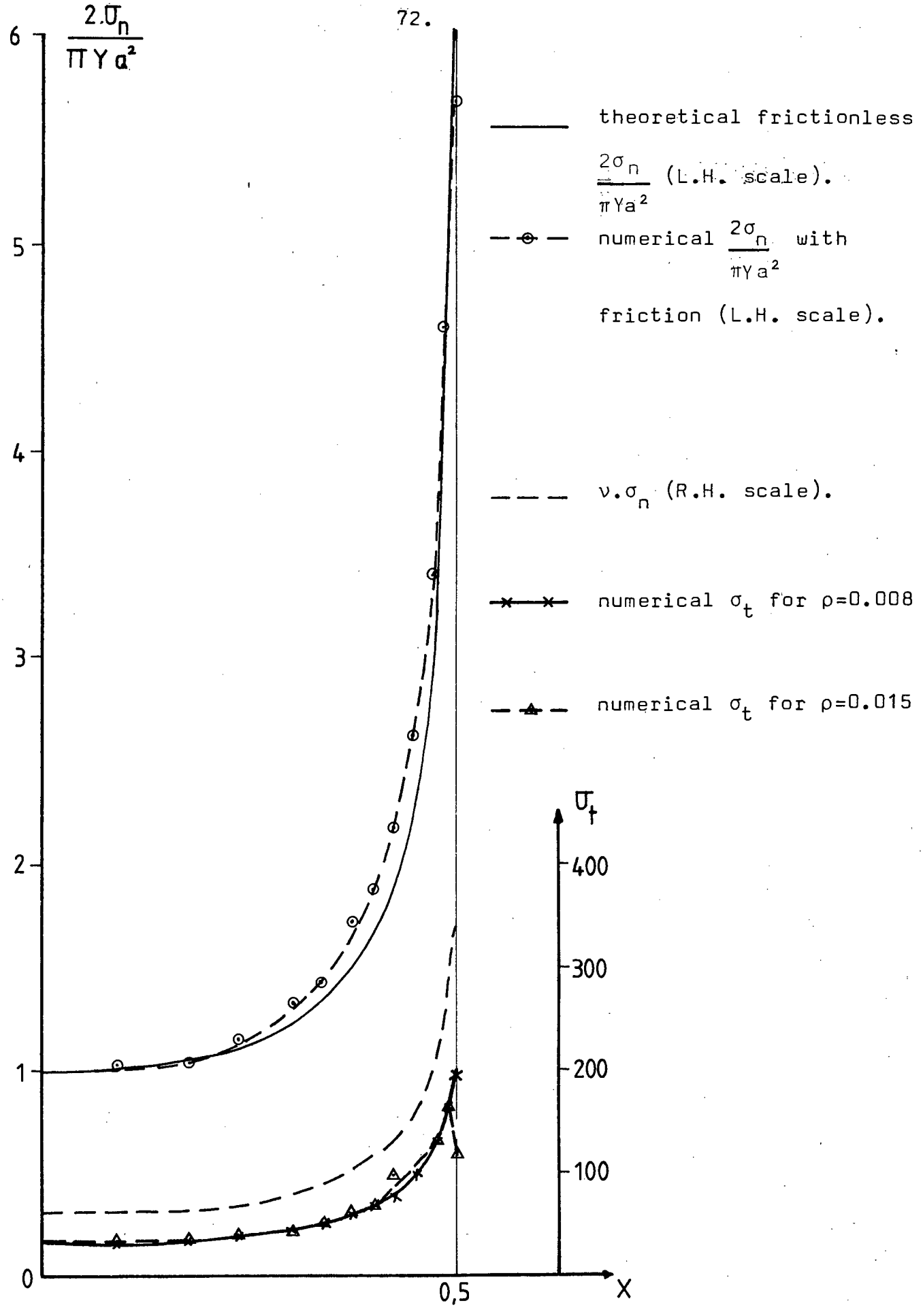

Figure 4.12. Normal and tangential stress profiles on the contact surface for the example of the rigid cylindrical punch on its end.

For the given indentation, the normal stresses along the frictional boundary were calculated and plotted against the theoretical solution given by Green and Zerna[19] for the frictionless contact problem (see Figure 4.12).

The tangential stress was also calculated for this indentation and varying ρ. (ρ varied from 0.008 to 0.015). The example also shows how, as $\rho \to 0$ the tangential stress tends to peak in a way similar to the normal stress, but as ρ is increased, the peak is reduced (see Figure 4.12).

4.3. Plane Stress Example

(i) A thin elastic sheet pulled through an opening

This problem consists of a thin elastic sheet of thickness 0.02 units, which is pulled in such a manner that a section of its free edge comes into contact with a rigid boundary. The sheet has a value of Young's modulus of 1000 units and Poisson's ratio of 0.3. The properties of the frictional boundary of the sheet are :

$$\nu = 0.3 \quad ,$$
$$0.01 \leq \rho \leq 0.1 \quad ,$$
$$\varepsilon = 10^{-4} \quad .$$

The finite element mesh for this example is given in Figure 4.13. This mesh consists of 24 8-noded isoparametric elements. The deformed shape is shown in Figure 4.14 for when the sheet

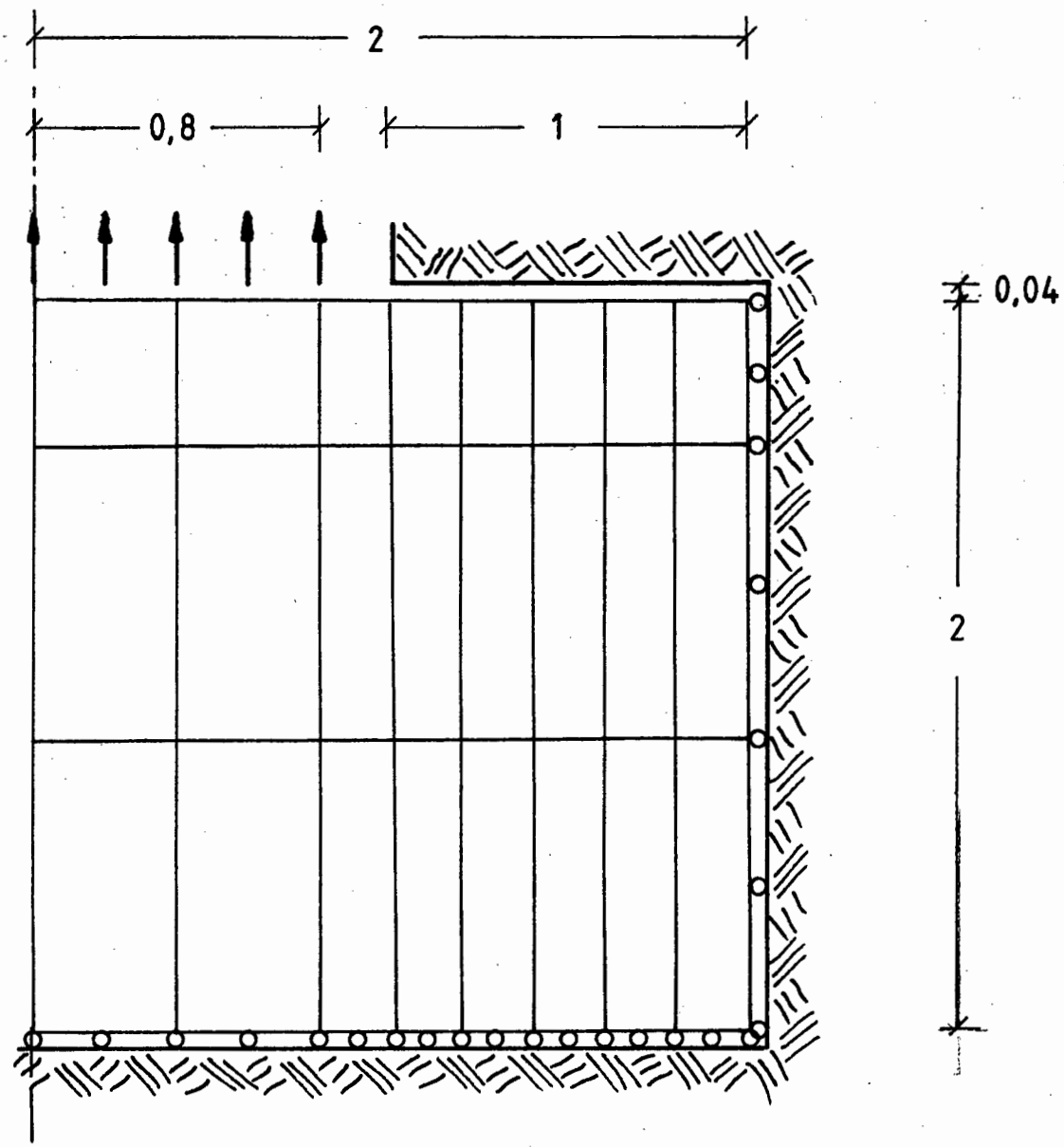

Figure 4.13. The finite element mesh for the example of the thin sheet being pulled through an opening.

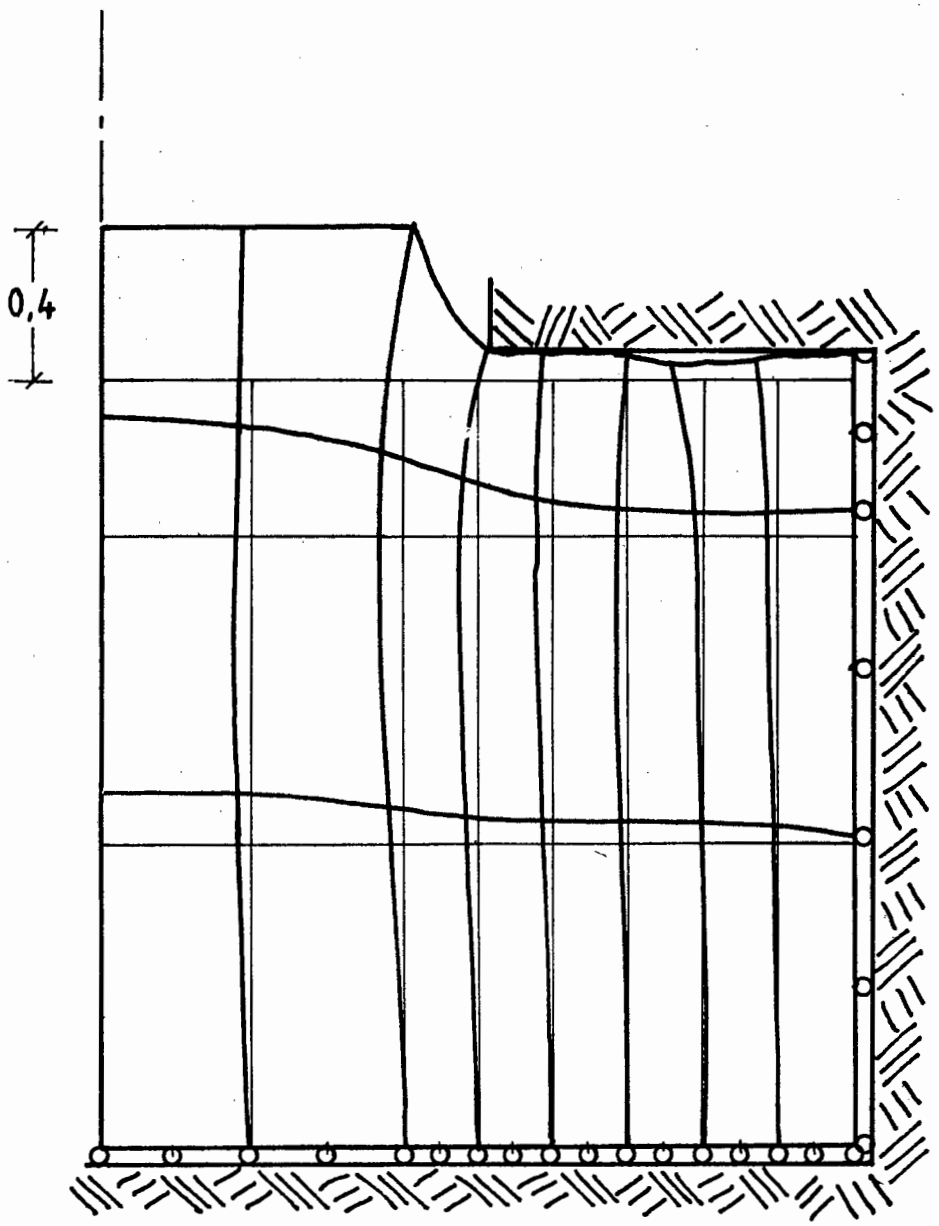

Figure 4.14. The computed deformed configuration for the thin sheet being pulled by 0.4 units.

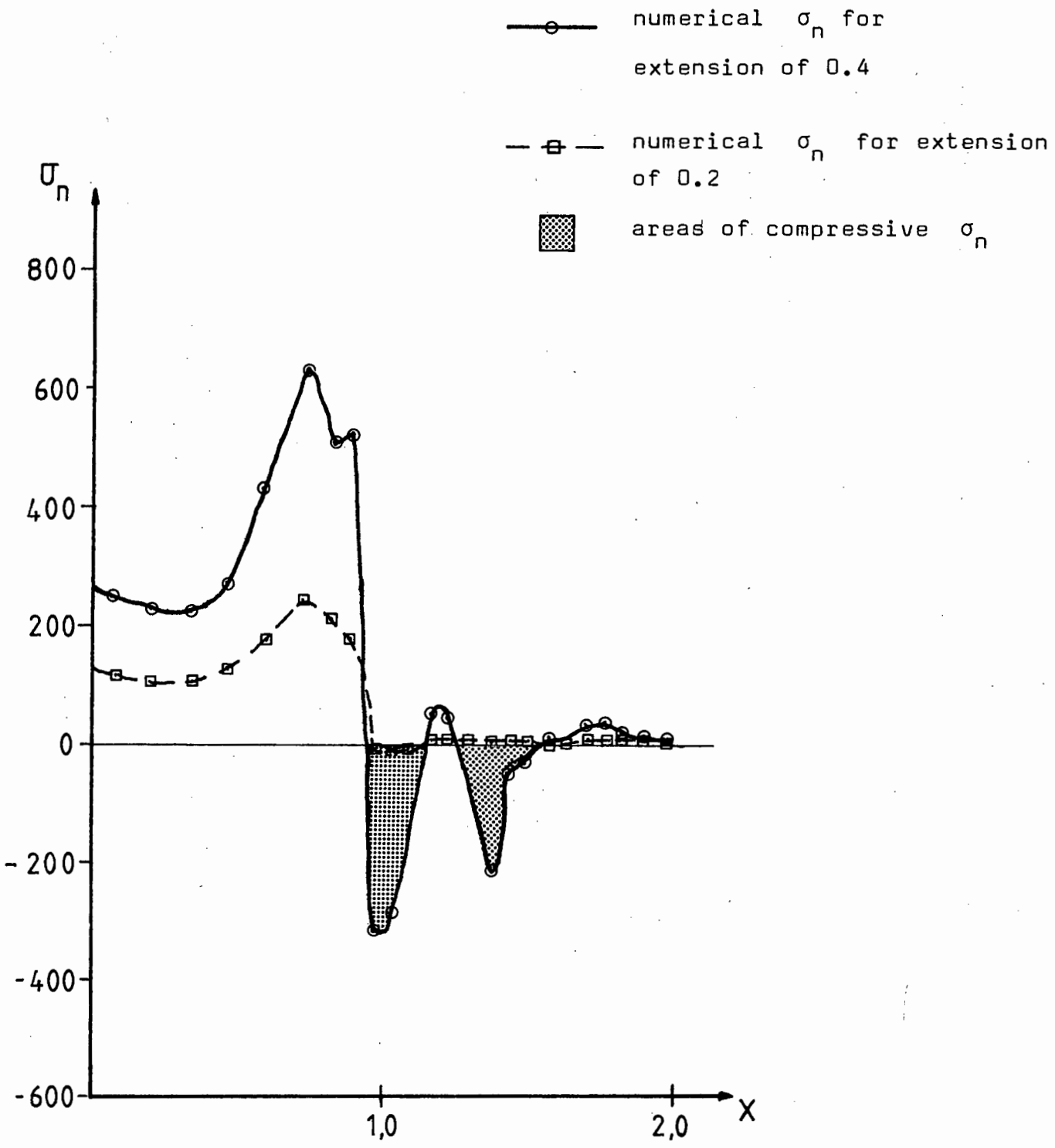

Figure 4.15. Normal stresses for an extension of 0.2 and 0.4 along the row of gauss points closest to the free edge.

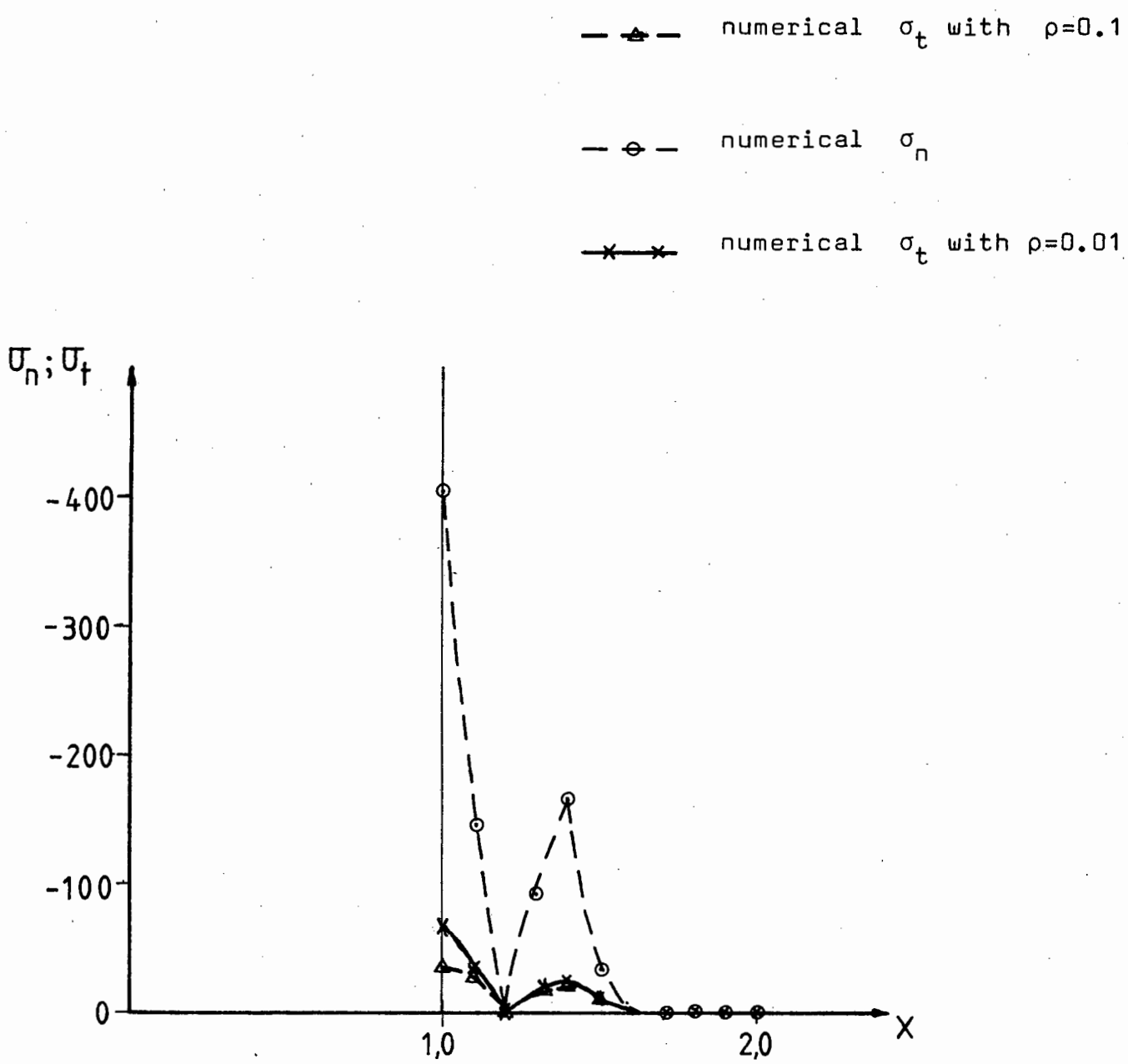

Figure 4.16. Normal and tangential stress profiles on the contact surface for the plane stress example.

has been pulled out by 0.4 units.

The normal stress along the closest row of gauss points to the boundary for an extension of 0.2 units and 0.4 units is given in Figure 4.15. This shows the distinct regions of tensile and compressive normal stress. For an extension of 0.2 units, the regions of compression along the possible contact edge are not clearly defined. Only when the extension reaches a value of 0.4 units do the compression regions become evident.

In Figure 4.16 the normal stress and tangential stress for $\rho=0.01$ and $\rho=0.1$ along the contact boundary are plotted. Again, it is seen that as $\rho\to 0$ the tangential stress tends to peak in a similar way to the normal stress.

CHAPTER FIVE

CONCLUSIONS

In this thesis a finite element approximation has been developed for contact problems in elasticity, using the non-classical friction law developed by Oden and Pires[1]. The element used is the standard 8-noded isoparametric element. The algorithm has been written in such a way that only two aspects of a standard finite element program for elastic problems need alteration, the first being the adjustment of the load vector to take into account the tangential frictional forces, and the second being the iterative scheme for obtaining the correct contact area and surface tractions on the possible area of contact.

The implementation in a standard finite element program, although satisfactory, has been found not to be ideal. For example, there is a lack of flexibility in the integration procedure to find the weighted normal stress on the boundary, since the integrations are performed along the edges of elements and account has to be taken of the extent of the function ω_ρ. A preferable scheme would be to free these integrations entirely from the constraints of the finite element mesh, so that the procedure for integration does not depend at all on the magnitude of the parameter ρ. Of course, the advantages of a non-standard program which includes these modifications have to be weighed against the efficiency of a slightly modified, but otherwise standard program such as the one implemented here.

Some aspects of the numerical results are also worth discussing. For punches with sharp edges there is a stress concentration with regard to the normal stress at the edges, and, if Coulomb friction is assumed, then there is a similar stress concentration with regard to the tangential stress. The major effect of the use of the nonlocal friction law is to cause a considerable reduction in the peak of tangential stress. For punches which do not have sharp edges, this reduction is not evident as stress concentrations do not occur.

The nonlinear parameter ε has not been varied in the examples given as its main function has been to regularise the curve of tangential stress vs. displacement (see Figure 1.4) from a discontinuous, non-differentiable stick/slide function to a continuous, differentiable elastic/sliding function. If $\varepsilon \to 0$ then the curve approaches the stick/slide function. Apart from this aspect, which is important from the numerical point of view, it is not expected that ε would have any appreciable effect on the results.

An area which will require attention is the extension of the friction law to one which is path-dependent. The present formulation as given by Oden and Pires [1] is path-independent, in that the solution for a given load is independent of the previous history. What would be required is a modification of this formulation so that it is cast in terms of incremental quantities, the value of these quantities depending amongst other things on the state

of the body at the moment at which the increment is considered. There are obvious analogies between this extension and the conventional formulation of constitutive equations in plasticity.

REFERENCES

1. Oden, J.T. and Pires, E.B.- Nonlocal and Nonlinear Friction Laws and Variational Principles for Contact Problems in Elasticity. J. Appl. Mech. 50 (1983) 67-76.

2. Campos, L.T., Oden, J.T. and Kikuchi, N. - A Numerical Analysis of a Class of Contact Problems with Friction in Elastostatics. Comp. Meth. Appl. Mech. Engng 34 (1982) 821-845.

3. Oden, J.T. and Pires, E.B.- Numerical Analysis of Certain Contact Problems in Elasticity with Non-classical Friction Laws. Comput. Struct. 16 (1982) 481-485.

4. Goldsmith, W. - Impact (Chapter 4: The Hertz Law of Contact) Edward Arnold (London) 1960.

5. Aleksandrova, G.P. - A Contact Problem Solved in Closed Form, on the Theory of Elasticity for a Cylindrical Body. Inzhenernyi Zhurnal Mekhanika Tverdogo Tela 2 (1968) 143-153.

6. Gladwell, G.M.L. - Contact Problems in the Classical Theory of Elasticity. Sijthoff and Noordhoff (Leyden) 1980.

7. Signorini, A. - Questioni di Elasticità non Linearizzata o Semi-linearizzata. Rend. di Matem. e delle sue appl. 18 (1959).

8. Fichera, G. - Problemi Elastostatici con Vincoli Unilaterale; il Probleme di Signorini con Ambigue Condizioni al Contorno. Mem. Accad. Naz. Lincei Ser. 8 7 (1964) 91-140.

9. Duvaut, G. and Lions, J.L. - Inequalities in Mechanics and Physics. Springer-Verlag (Berlin) 1976.

10. Kalker, J.J. - Numerical Contact Elastostatics. Variational Methods in the Mechanics of Solids (ed. S. Nemat-Nasser) Pergamon (Oxford) (1978) 242-248.

11. Kalker, J.J. - A Minimum Principle for the Law of Dry Friction with Application to Elastic Cylinders in Rolling Contact, part I and part II. J. Appl. Mech. 38 (1971) 875-887.

12. Kalker, J.J. - Variational Principles of Contact Elastostatics. J. Inst. Maths. Applics. 20 (1977) 199-219.

13. Kalker, J.J. - On Elastic Contact. J. Appl. Mech. 39 (1972) 1125-1132.

14. Kalker, J.J. - The Surface Displacement of an Elastic Half-space Loaded in a Slender Curved Bounded Region with Application to the Calculation of the Contact Pressure under a Roller. J. Inst. Maths. Applic. 19 (1977) 127-144.

15. Kalker, J.J. and Panek, C. - A Solution for the Narrow Rectangular Punch. J. Elast. 7 (1977) 213-218.

16. Singh, K.P. and Paul, B. - Numerical Solution of Non-Hertzian Elastic Contact Problems. J. Appl. Mech. 41 (1974) 484-490.

17. Conry, T.F. and Siereg, A. - Mathematical Programming Method for Design of Elastic Bodies in Contact. J. Appl. Mech. 38 (1971) 387-392.

18. Francavilla, A. and Zienkiewicz, O.C. - A Note on Numerical Computation of Elastic Contact Problems. Int. J. Num. Meth. Engng 9 (1975) 913-924.

19. Green, A.E. and Zerna, W. - Theoretical Elasticity, Second Edition. Oxford University Press (Oxford) 1964.

20. Little, R.Wm. - Elasticity. Prentice-Hall (New Jersey) 1973.

21. Sneddon, I.N. - Fourier Transforms. McGraw-Hill (New York) 1951.

22. Bowden, F.P. and Tabor, D. - The Friction and Lubrication of Solids, Vols. 1 and 2. Oxford University Press (Oxford) 1964.

23. Bathé, K.-J. - Finite Element Procedures in Engineering Analysis. Prentice-Hall (New Jersey) 1982.

24. Becker, E.B., Carey, G.F. and Oden, J.T. - Finite Elements: Vol. 1, an Introduction. Prentice-Hall (New Jersey) 1981.